arXiv:1610.09206v1 [quant-ph] 28 Oct 2016

Controlled-phase gate for photons based on stationary light

Ivan Iakoupov[1], Johannes Borregaard[1,2], and Anders S. Sørensen[1]
[1] *The Niels Bohr Institute, University of Copenhagen, Blegdamsvej 17, DK-2100 Copenhagen Ø, Denmark*
[2] *Department of Physics, Harvard University, Cambridge, MA 02138, USA*
(Dated: October 31, 2016)

We propose a method to induce strong effective interactions between photons mediated by an atomic ensemble. To achieve this, we use the stationary light effect, which makes the atomic ensemble behave as an optical cavity and thereby increases the interaction strength. Regardless of the optical depth per atom, the interaction strength between the photons can be enhanced by increasing the total number of atoms (total optical depth). For sufficiently many atoms, the setup can be viable as a controlled-phase gate for photons. We derive analytical expressions for the fidelities for two modes of gate operation: deterministic and heralded conditioned on the presence of two photons at the output. The latter mode can be used to improve the secret key rate for quantum repeaters compared to using only linear optics.

Optical photons are ideal carriers of quantum information over long distances, and such quantum communication may enable a wealth of applications [1]. Quantum information processing with photonic qubits is, however, severely limited by the lack of efficient two-qubit gates. In principle, such gates could be realized by strongly coupling photons to a single atom [2, 3]. Experiments have pushed towards realizing such strong coupling, e.g. in cavity QED structures [4–8] and optical waveguides [9–12], but the realization of gates remains challenging. An alternative approach to strong light-matter interactions is to use atomic ensembles where a large number of atoms compensates for a small coupling efficiency of the individual atoms [13], but this approach typically does not enhance the nonlinear interactions required for quantum gates. In recent years, experiments in e.g. tapered optical fibers [14–18] and hollow core photonic-crystal fibers [19, 20] have realized an intermediate regime where the coupling of the individual atoms is sizeable, but still not sufficient to realize photonic gates based on single atoms. It is thus an open question to which degree such moderate couplings enable processing of quantum information.

In this letter, we propose a method to exploit the moderate coupling regime to realize quantum gates between photons. We show that by using sufficiently many atoms it is possible to compensate for the limited coupling strength of the individual atoms and achieve ideal gate operation [22]. The proposed gate is based on *stationary light* [23–25] where polaritons (coupled light-matter excitations) have very low group velocity due to counter-propagating classical drives. Reflections from the ends of an ensemble experiencing stationary light result in a cavity-like transmission spectrum with transmission resonances whenever the polaritons form standing waves inside the ensemble [22]. We show that the storage of a single photon completely changes the transmission spectra of the ensemble, see Fig. 1(a), because the cavity structure created by the remaining atoms enhances the interaction with the stored excitation. This can be used to mediate a gate between photons, which can be either deterministic or heralded where successful operation is conditioned on subsequent detection of two photons. As a particular application we show that the gate can be directly used to enhance the communication rate of en-

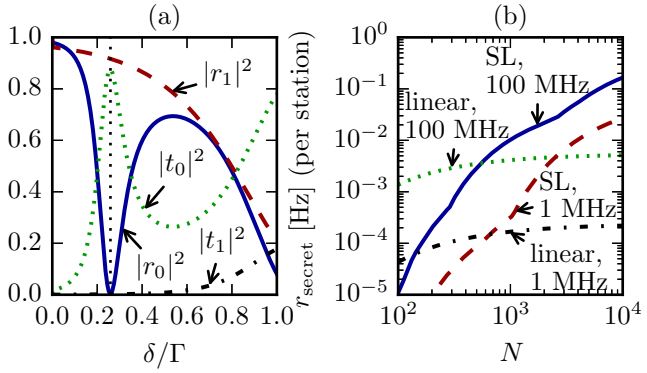

FIG. 1. (Color online) (a) Reflectances ($|r_0|^2$, $|r_1|^2$) and transmittances ($|t_0|^2$, $|t_1|^2$) of an ensemble of Λ-type atoms without ($|r_0|^2$, $|t_0|^2$) and with ($|r_1|^2$, $|t_1|^2$) a stored photon for different frequencies (two-photon detunings) δ in units of the total linewidth Γ. The vertical dotted line marks the operation point. The parameters are: number of atoms $N = 1000$, $\Gamma_{1D}/\Gamma = 0.5$, $\Delta_c/\Gamma = -16$, and $\Omega_0/\Gamma = 10$. (b) Secret key rate $r_{\rm secret}$ per repeater station as a function of the number of atoms N with fixed $\Gamma_{1D}/\Gamma = 0.5$ for dual-V atoms and a communication distance of 1000 km. We compare the protocol of Ref. [21] ("linear") with a modified protocol where the entanglement swapping (and also initial entanglement generation if it improves $r_{\rm secret}$) is performed with the proposed stationary light CP gate ("SL"). We consider two different source repetition rates: 100 MHz and 1 MHz. We assume an attenuation length of 22 km in the fibers and an optical signal speed of 2×10^5 km/s. The ensemble storage and retrieval efficiency increases with N and is set to the same value in the original protocol as for the modified one. The photodetector efficiency is assumed to be 90%. The steps in the curves occur when the fidelity of the CP gate allows additional swap levels.

semble based quantum repeaters [21, 26, 27] (Fig. 1(b)).

Overview. We consider two different level schemes for the atoms in the ensemble: Λ-type and dual-V (Figs. 2(a) and 2(b), respectively). The linear properties of these two schemes are described in detail in Ref. [28]. In the Λ-type scheme, the two classical drives have the same polarization, which results in a standing wave of the Rabi frequency $\Omega(z) = \Omega_0 \cos(k_0 z)$, where k_0 is the wave vector of the classical drive, assumed to be the same as the wave vector of the probe field $\hat{\mathcal{E}}_\pm$ (single photon). For the Λ-type scheme, we assume that the atoms are placed at positions $z_j = j\pi/(2k_0)$ with $0 \le j \le N-1$ to achieve the lowest possible group velocity [28]. This scheme is easier to analyze, and all our analytical results are obtained for this scheme. The dual-V scheme [25, 29] is less sensitive to the exact positions of the atoms and hence easier to implement in practice. For the dual-V scheme, we only verify numerically that the gate errors have the same scaling as for the Λ-type scheme.

The coupling of the atoms to the waveguide is characterized by the parameter Γ_{1D}/Γ (half of the optical depth per atom), where Γ_{1D} is the decay rate from state $|b\rangle$ for the Λ-type scheme into both right-moving and left-moving guided modes (assumed to be equal), Γ' is the decay rate into all the other modes, and $\Gamma = \Gamma_{1D} + \Gamma'$ is the total decay rate. In the dual-rail encoding of photonic qubits shown in Fig. 2(c), two identical atomic ensembles are required, where the upper one only functions as a memory. Alternatively, the single-rail encoding can also be implemented with one atomic ensemble [30], but the dual-rail encoding allows heralded operation, which has better fidelity. Each ensemble is placed inside a Sagnac interferometer (Fig. 2(d)).

The operation of the CP gate is sequential. First, photon A is stored either in the upper ($|0\rangle_A$) or the lower ($|1\rangle_A$) ensemble using electromagnetically induced transparency (EIT) [31]. Then photon B is scattered from the lower ensemble under conditions of stationary light ($|1\rangle_B$) or passes through a beam splitter with transmission coefficient t_b ($|0\rangle_B$). The role of this beam splitter will be explained below. The Sagnac interferometer can be set up such that most of the incident power in each of its two input ports is reflected back through the same port, regardless of whether the ensemble is reflective or transmissive. Reflection or transmission of the ensemble instead controls the phase of the reflected field. The scattering of photon B can be arranged such that if there is no stored photon in the lower ensemble (photon A is in the state $|0\rangle_A$), the atomic ensemble is completely transmissive in the ideal case, and photon B is reflected from the Sagnac interferometer with no additional phase. If there is a stored photon (photon A is in state $|1\rangle_A$), photon B is reflected from the interferometer with a π phase shift. The latter case performs the desired controlled-phase gate operation $|11\rangle_{AB} \to -|11\rangle_{AB}$, while the rest of the basis states are unchanged. Finally, photon A is retrieved using EIT.

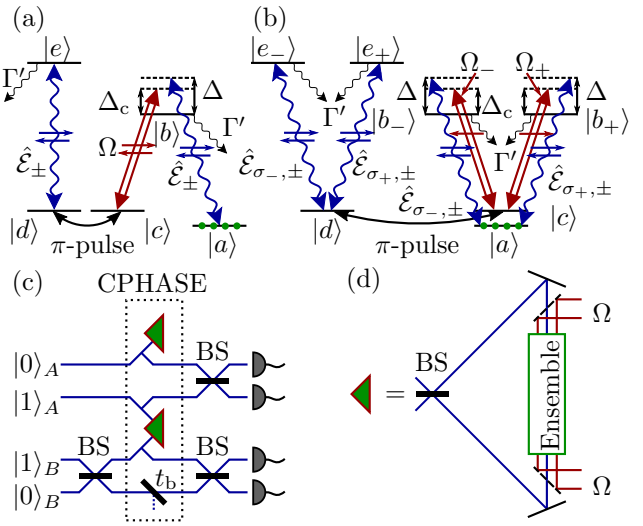

FIG. 2. (Color online) (a) Level diagram of a Λ-type atom (levels $|a\rangle$, $|b\rangle$, and $|c\rangle$), which can be switched to a two-level atom (levels $|d\rangle$ and $|e\rangle$) by the storage of a photon followed by a π-pulse. The green dots indicate the initial state of the atoms. (b) Level diagram of a dual-V atom which can be switched to a V-type atom. (c) A dual-rail Bell-state measurement setup with the controlled-phase gate (labeled by CPHASE) as a part of it. An ensemble of atoms is placed inside a Sagnac interferometer, shown as a triangle in (c) and defined by (d). In the rail corresponding to state $|0\rangle_B$, a beam splitter is added with transmission coefficient t_b. All the other beam splitters (BS) are 50:50.

Storage and retrieval. Under EIT storage and retrieval, the incident photon is resonant with the classical drive, and the classical drive is incident from one side and is assumed to be resonant with its transition for simplicity. After entering the Sagnac interferometer, photon A will be split into two halves by the 50:50 beam-splitter (see Fig. 2(d)), which upon reaching the ensemble from the opposite sides will have opposite spatial phase factors $e^{ik_0 z}$ and $e^{-ik_0 z}$ and interfere inside the ensemble resulting in a spatially modulated $\cos(k_0 z)$ stored spin wave. Such storage procedure is necessary for the Λ-type scheme, since the part of the excitation that is stored on the nodes of the standing wave of the classical drive (that is applied during scattering of photon B) does not change the scattering properties of the ensemble. Before the EIT storage, all atoms are initialized in state $|a\rangle$, and after storage, the incident photon is mapped onto an atom being in state state $|c\rangle$. To produce an optical non-linearity, we assume that state $|c\rangle$ is subsequently transferred to state $|d\rangle$ using a π-pulse.

Reflection and transmission. We use the (multi-mode) transfer matrix formalism [28, 32] to model the scattering process. To illustrate the scattering behavior, we assume that photon A was stored in the center of the atomic

ensemble at an anti-node of the classical drive. The reflectances and transmittances of an ensemble of Λ-type atoms are plotted in Fig. 1(a) as functions of two-photon detuning $\delta = \Delta - \Delta_c$, where Δ (Δ_c) is the detuning of the probe field (classical drive). The reflectance $|r_0|^2$ ($|r_1|^2$) and transmittance $|t_0|^2$ ($|t_1|^2$) are for an ensemble without (with) a stored photon. The ensemble is seen to have transmittance resonances with a large transmittance and a small reflectance, similar to the transmission of a cavity. These resonances occur when the standing wave condition is fulfilled, i.e. $\sin(qL) = 0$, where q is the Bloch vector of the stationary light polaritons and L is the length of the ensemble [22, 28]. When a photon is stored in the ensemble, an atom changes from state $|a\rangle$ to $|d\rangle$. In state $|d\rangle$, the atom acts as a two-level atom that is resonant with the incident photon (see Fig. 2(a)). Since the effective interaction is enhanced by the cavity-like behavior of the ensemble, this single two-level atom can have a strong effect of an incident photon, even though the atom in itself has a limited coupling.

We focus on the behavior at the resonance nearest $\delta = 0$ (vertical dotted line in Fig. 1(a)). In the limit of large atom number N and for $|\Delta_c| \neq 0$, this resonance is at a two-photon detuning $\delta_{\rm res} \approx -4\Delta_c\pi^2|\Omega_0|^2/(\Gamma_{1D}^2 N^2)$, for which we obtain [29]

$$r_0 \approx \frac{\Gamma_{1D}\Gamma' N}{16\Delta_c^2} + \frac{\Gamma'|\Omega_0|^2\pi^2}{2\Delta_c^2\Gamma_{1D}N}, \tag{1}$$

$$t_0 \approx 1 - r_0, \tag{2}$$

$$r_1(\tilde{z}) \approx 1 - \frac{4\pi^2\Gamma'\Delta_c^2}{\Gamma_{1D}^3N^2} + \frac{32\pi^4\Delta_c^2\Gamma'|\Omega_0|^2}{\Gamma_{1D}^5N^4} - \frac{4i\pi^2\Delta_c}{\Gamma_{1D}N}\left(\tilde{z}-\frac{1}{2}\right) - \frac{4\pi^4\Delta_c^2(2\Gamma_{1D}+\Gamma')}{\Gamma_{1D}^3N^2}\left(\tilde{z}-\frac{1}{2}\right)^2, \tag{3}$$

$$t_1(\tilde{z}) \approx \frac{4\pi^2\Delta_c^2\Gamma'}{\Gamma_{1D}^3N^2} - \frac{32\pi^4\Delta_c^2\Gamma'|\Omega_0|^2}{\Gamma_{1D}^5N^4} + \frac{8\pi^4\Delta_c^2\Gamma'}{\Gamma_{1D}^3N^3}\left(\tilde{z}-\frac{1}{2}\right) + \frac{4\pi^4\Delta_c^2\Gamma'}{\Gamma_{1D}^3N^2}\left(\tilde{z}-\frac{1}{2}\right)^2. \tag{4}$$

Here, t_1 and r_1, were obtained by solving the discrete problem, where a photon is stored in a single discrete atom and then taking the continuum limit such that the index of the atom is replaced by its position inside the ensemble $\tilde{z} = z/L$. The Ω_0 dependent terms are only relevant for determining the gate time and will be ignored for now. By aligning the interferometer, the reflection coefficients of the combined interferometer-ensemble system are given by $R_0 = -(r_0 - t_0)$ and $R_1(\tilde{z}) = -(r_1(\tilde{z}) - t_1(\tilde{z}))$ [29]. If we take $\tilde{z} = 1/2$ and a detuning $|\Delta_c| \sim \Gamma_{1D}N^{3/4}$, we have $r_0, t_1 \sim \Gamma'/(\Gamma_{1D}\sqrt{N})$, $r_1 \approx 1 - t_1$, and $t_0 \approx 1 - r_0$. Hence, regardless of the value of Γ'/Γ_{1D} we can achieve an ideal CP gate $R_0 = 1$, $R_1 = -1$ with sufficiently many atoms.

Fidelity. To quantify the errors of the gate, we calculate the Choi-Jamiolkowski (CJ) fidelity [30]. The EIT storage is described using the storage K_s and retrieval K_r kernels derived in Ref. [31] (suitably modified to take into account storage from both directions [29]). When photon A is stored and retrieved without a scattering taking place, its wave function is $\phi_{A,\text{out},0}(t) = \int\int K_r(\tilde{z},t)K_s(\tilde{z},t')\phi_{A,\text{in}}(t')\,\mathrm{d}t'\,\mathrm{d}\tilde{z}$, where $\phi_{A,\text{in}}$ is the wave function of the input photon A. The efficiency of the storage and retrieval is then $\eta_{\rm EIT} = \int|\phi_{A,\text{out},0}(t)|^2\,\mathrm{d}t$. If photon B was reflected from the interferometer, while photon A was stored in the ensemble (computational basis state $|11\rangle_{AB}$), the wave function of the retrieved photon A is instead $\phi_{A,\text{out},1}(t) = \int\int K_r(\tilde{z},t)R_1(\tilde{z})K_s(\tilde{z},t')\phi_{A,\text{in}}(t')\,\mathrm{d}t'\,\mathrm{d}z$. Neglecting bandwidth effects of photon B, we obtain the CJ fidelity

$$F_{\rm CJ} = \frac{\eta_{\rm EIT}}{16}\left|2t_b + R_0 - R_{1,1}\right|^2, \tag{5}$$

where $R_{1,1} = (1/\eta_{\rm EIT})\int\phi^*_{A,\text{out},0}(t)\phi_{A,\text{out},1}(t)\,\mathrm{d}t$. If the gate is conditioned on the presence of two photons after the gate operation [30, 33, 34], we find that the success probability is

$$P_{\rm suc} = \frac{\eta_{\rm EIT}}{4}\left(2|t_b|^2 + |R_0|^2 + R_{1,2}\right), \tag{6}$$

with $R_{1,2} = (1/\eta_{\rm EIT})\int|\phi_{A,\text{out},1}(t)|^2\,\mathrm{d}t$, and the conditional CJ fidelity is $F_{\rm CJ,cond} = F_{\rm CJ}/P_{\rm suc}$.

To optimize the performance of the gate, we set $t_b = 1$ and optimize Δ_c and the width of the stored spin wave $\tilde{\sigma} = \sigma/L$ such that $F_{\rm CJ}$ is maximal. Afterwards, for fixed optimal Δ_c and $\tilde{\sigma}$ we explore the effect of $t_b < 1$. As shown below, $F_{\rm CJ,cond}$ can be substantially improved by choosing a particular $t_b < 1$ at the cost of increasing $1 - P_{\rm suc}$ by a constant factor. Whether this is a desirable trade off, depends on the particular application. In Fig. 3(a) we plot the numerically calculated $F_{\rm CJ} \approx P_{\rm suc}$ and $F_{\rm CJ,cond}$ for the Λ-type scheme, where photon A was chosen to have a Gaussian temporal profile, and photon B is centered on $\delta = \delta_{\rm res}$ and assumed to be narrow in frequency compared to the resonance width. As seen in the figure, both $F_{\rm CJ}$ and $F_{\rm CJ,cond}$ approach their ideal value of unity for large N, but $F_{\rm CJ,cond}$ approaches it much faster.

For large N, we can find analytical expressions for the curves in Fig. 3(a). The stored spin wave will be approximately Gaussian so that it has the form $S(\tilde{z}) = (2\pi\tilde{\sigma}^2)^{-1/4}\exp\left(-(\tilde{z}-1/2)^2/(4\tilde{\sigma}^2)\right)$. Consequently, $\eta_{\rm EIT} \approx 1 - \Gamma'/(2N\Gamma_{1D}\tilde{\sigma}^2)$ [29]. Neglecting distortions of photon A under storage and retrieval, but still accounting for errors due to the spatial extent of the stored excitation, we approximate $R_{1,1} \approx \int R_{1,s}(\tilde{z})|S(\tilde{z})|^2\,\mathrm{d}\tilde{z}$ and $R_{1,2} \approx \int|R_{1,s}(\tilde{z})|^2|S(\tilde{z})|^2\,\mathrm{d}\tilde{z}$. Here, $R_{1,s}(\tilde{z}) = (R_1(\tilde{z}) + R_1(1-\tilde{z}))/2$ is a symmetrized version of R_1, which accounts for storage and scattering from both sides of the ensemble due to the Sagnac interferometer.

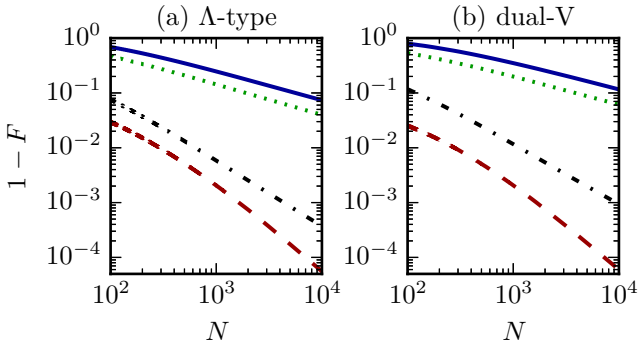

FIG. 3. (Color online) (a) Numerically calculated fidelities for the Λ-type scheme. For $t_\mathrm{b}=1$, $F_\mathrm{CJ}\approx P_\mathrm{suc}$ and $F_\mathrm{CJ,cond}$ are shown by dotted green and dash-dotted black curves respectively. For $t_\mathrm{b}<1$ chosen such that $F_\mathrm{CJ,cond}$ is maximal, $F_\mathrm{CJ}\approx P_\mathrm{suc}$ and $F_\mathrm{CJ,cond}$ are shown by solid blue and dashed red lines respectively. (b) The same as in (a), but using the dual-V instead and interatomic spacing $d=0.266\pi/k_0$. The common parameters are $\Gamma_\mathrm{1D}/\Gamma=0.5$, and $\Omega_0/\Gamma=1$. Under EIT (storage and retrieval), $\Omega(z)=\Omega_0$. Under stationary light (scattering), $\Omega(z)=\Omega_0\cos(k_0z)$ and $\Omega_\pm(z)=\Omega_0e^{\pm ik_0z}$ for Λ-type and dual-V respectively.

For fixed Γ_1D and large N, after choosing $\tilde{\sigma}^2=1/(\pi^{3/2}N^{1/4})\sqrt{\Gamma'/(\Gamma_\mathrm{1D}+\Gamma')}$, $\Delta_\mathrm{c}^2=(\Gamma_\mathrm{1D}^2N^{3/2})/(8\pi)$, and $t_\mathrm{b}=1$, such that F_CJ is maximal, we get

$$F_{\mathrm{CJ},t_\mathrm{b}=1}\approx P_{\mathrm{suc},t_\mathrm{b}=1}\approx 1-\frac{\pi\Gamma'}{\Gamma_\mathrm{1D}\sqrt{N}}, \tag{7}$$

$$F_{\mathrm{CJ,cond},t_\mathrm{b}=1}\approx 1-\frac{\pi^2\Gamma'^2}{4\Gamma_\mathrm{1D}^2N}. \tag{8}$$

If $t_\mathrm{b}=R_0$, $F_\mathrm{CJ,cond}$ is maximal, and we get

$$F_{\mathrm{CJ},t_\mathrm{b}=R_0}\approx P_{\mathrm{suc},t_\mathrm{b}=R_0}\approx 1-\frac{2\pi\Gamma'}{\Gamma_\mathrm{1D}\sqrt{N}}, \tag{9}$$

$$F_{\mathrm{CJ,cond},t_\mathrm{b}=R_0}\approx 1-\frac{11\pi^3\left(\Gamma_\mathrm{1D}+\Gamma'\right)\Gamma'}{16\Gamma_\mathrm{1D}^2N^{3/2}}. \tag{10}$$

These expressions confirm that the gate fidelity improves with N and that the conditional fidelities have better scaling.

In Fig. 3(b) we plot the numerically calculated fidelities F_CJ and $F_\mathrm{CJ,cond}$ for the dual-V scheme. In the simulation, the distance between the atoms was set to be incommensurate with the wavelength of the classical drive $d=0.266\pi/k_0$. The results are, however, almost independent of d, and the gate can function even with completely random placement of the atoms [29]. The dual-V scheme is seen to have a very similar behavior to the Λ-type scheme.

Gate time. The gate time will be set both by the storage and retrieval time of photon A and the necessity of the scattered photon B to be narrow in frequency. The EIT storage and retrieval time is limited by $1/(\Gamma_\mathrm{1D}N)$ [31] and decreases with larger N. We therefore focus on the scattering of photon B.

Due to non-zero bandwidth of photon B, the reflection coefficient R_0 (at $\delta=\delta_\mathrm{res}$) in Eq. (5) should be replaced by $\int R_0(\delta)|\phi_B(\delta)|^2\,\mathrm{d}\delta$ [29], where ϕ_B is the frequency distribution of photon B. Since r_1 and t_1 vary much slower than r_0 and t_0 around $\delta=\delta_\mathrm{res}$ (vertical dotted line in Fig. 1(a)), we ignore a similar modification to $R_{1,1}$ in Eq. (5).

We first expand the reflection coefficient r_0 around δ_res. We thereby obtain $r_0(\delta)\approx(2/w^2)(\delta-\delta_\mathrm{res})^2+r_0(\delta_\mathrm{res})$ with $w=(32\sqrt{2}\Delta_\mathrm{c}^2|\Omega_0|^2\pi^2)/(\Gamma_\mathrm{1D}^3N^3)$ being the resonance width. Defining the spectral width of photon B by $\sigma_B=\int(\delta-\delta_\mathrm{res})^2|\phi_B(\delta)|^2\,\mathrm{d}\delta$, we get $\int R_0(\delta)|\phi_B(\delta)|^2\,\mathrm{d}\delta\approx R_0(\delta_\mathrm{res})-(4/w^2)\sigma_B^2$. We now include the Ω_0 dependent terms in Eqs. (1) and (2). For optimal $|\Omega_0|^2=(\Gamma_\mathrm{1D}^{5/3}N^{11/6}\sigma_B^{2/3})/(2^{5/3}\pi^{5/3}\Gamma'^{1/3})$, we get $F_{\mathrm{CJ},t_\mathrm{b}=1,\sigma_B}\approx F_{\mathrm{CJ},t_\mathrm{b}=1}-(3\pi^{4/3}\Gamma'^{2/3}\sigma_B^{2/3})/(2^{2/3}\Gamma_\mathrm{1D}^{4/3}N^{2/3})$. Requiring the error from finite bandwidth to be proportional to the error in Eq. (7), we find that the required time is $1/\sigma_B\sim 1/(\sqrt{\Gamma_\mathrm{1D}\Gamma'}N^{1/4})$. Hence, the gate time decreases with N.

Repeater secret key rate. As a direct application of the proposed CP gate, we consider quantum repeaters based on atomic ensembles [26, 27]. We modify one of the fastest known repeater protocols for atomic ensembles [21] by implementing the proposed CP gate instead of linear optics for entanglement swapping using the setup in Fig. 2(c). The secret key rate per repeater station is calculated as described in Ref. [35] and compared to the results of the original protocol (see Fig. 1(b)). This analysis is similar to the CP gate in Ref. [30] with the difference that we also consider the possibility of generating the initial entanglement using the CP gate. For a fair comparison, we consider equal storage and retrieval efficiencies for both protocols. As seen in Fig. 1(b) for $\Gamma_\mathrm{1D}/\Gamma=0.5$, the proposed gate allows improving the rate of quantum repeaters if $N\gtrsim 1000$.

Conclusion. We have shown, how stationary light can be used to create a CP gate between photons. Most importantly, the gate can exploit a large number of atoms N to compensate for a limited single-atom coupling efficiency to light. In particular, the gate can have a rapid convergence as $N^{-3/2}$ towards unit fidelity, if it is operated in a heralded fashion. The gate is ideally suited to be employed in setups currently under development [15–20], where there is a moderate coupling efficiency to light $\Gamma_\mathrm{1D}/\Gamma\sim 0.01-0.5$. The gate can be directly employed to improve the communication rate of quantum repeaters based on atomic ensembles and may in general serve as a tool for photonics based quantum information processing.

The research leading to these results was funded by the European Union Seventh Framework Programme through SIQS (Grant No. 600645) and ERC Grant QIOS

(Grant No. 306576). J.B. acknowledges funding from the Carlsberg foundation.

[1] H. J. Kimble, Nature **453**, 1023 (2008).
[2] L.-M. Duan and H. J. Kimble, Phys. Rev. Lett. **92**, 127902 (2004).
[3] D. E. Chang, A. S. Sorensen, E. A. Demler, and M. D. Lukin, Nat Phys **3**, 807 (2007).
[4] H. Kim, R. Bose, T. C. Shen, G. S. Solomon, and E. Waks, Nat Photon **7**, 373 (2013).
[5] W. Chen, K. M. Beck, R. Bücker, M. Gullans, M. D. Lukin, H. Tanji-Suzuki, and V. Vuletić, Science **341**, 768 (2013).
[6] T. G. Tiecke, J. D. Thompson, N. P. de Leon, L. R. Liu, V. Vuletić, and M. D. Lukin, Nature **508**, 241 (2014).
[7] B. Hacker, S. Welte, G. Rempe, and S. Ritter, Nature **536**, 193 (2016).
[8] J. Volz, M. Scheucher, C. Junge, and A. Rauschenbeutel, Nat Photon **8**, 965 (2014).
[9] A. V. Akimov, A. Mukherjee, C. L. Yu, D. E. Chang, A. S. Zibrov, P. R. Hemmer, H. Park, and M. D. Lukin, Nature **450**, 402 (2007).
[10] J. Claudon, J. Bleuse, N. S. Malik, M. Bazin, P. Jaffrennou, N. Gregersen, C. Sauvan, P. Lalanne, and J.-M. Gérard, Nat Photon **4**, 174 (2010).
[11] A. Goban, C.-L. Hung, S.-P. Yu, J. D. Hood, J. A. Muniz, J. H. Lee, M. J. Martin, A. C. McClung, K. S. Choi, D. E. Chang, O. Painter, and H. J. Kimble, Nat Commun **5** (2014).
[12] I. Söllner, S. Mahmoodian, S. L. Hansen, L. Midolo, A. Javadi, G. Kiršanskė, T. Pregnolato, H. El-Ella, E. H. Lee, J. D. Song, S. Stobbe, and P. Lodahl, Nat Nano **10**, 775 (2015).
[13] K. Hammerer, A. S. Sørensen, and E. S. Polzik, Rev. Mod. Phys. **82**, 1041 (2010).
[14] F. Le Kien, V. I. Balykin, and K. Hakuta, Phys. Rev. A **70**, 063403 (2004).
[15] E. Vetsch, D. Reitz, G. Sagué, R. Schmidt, S. T. Dawkins, and A. Rauschenbeutel, Phys. Rev. Lett. **104**, 203603 (2010).
[16] A. Goban, K. S. Choi, D. J. Alton, D. Ding, C. Lacroûte, M. Pototschnig, T. Thiele, N. P. Stern, and H. J. Kimble, Phys. Rev. Lett. **109**, 033603 (2012).
[17] J.-B. Béguin, E. M. Bookjans, S. L. Christensen, H. L. Sørensen, J. H. Müller, E. S. Polzik, and J. Appel, Phys. Rev. Lett. **113**, 263603 (2014).
[18] B. Gouraud, D. Maxein, A. Nicolas, O. Morin, and J. Laurat, Phys. Rev. Lett. **114**, 180503 (2015).
[19] M. Bajcsy, S. Hofferberth, V. Balic, T. Peyronel, M. Hafezi, A. S. Zibrov, V. Vuletic, and M. D. Lukin, Phys. Rev. Lett. **102**, 203902 (2009).
[20] F. Blatt, L. S. Simeonov, T. Halfmann, and T. Peters, Phys. Rev. A **94**, 043833 (2016).
[21] N. Sangouard, C. Simon, B. Zhao, Y.-A. Chen, H. de Riedmatten, J.-W. Pan, and N. Gisin, Phys. Rev. A **77**, 062301 (2008).
[22] M. Hafezi, D. E. Chang, V. Gritsev, E. Demler, and M. D. Lukin, Phys. Rev. A **85**, 013822 (2012).
[23] A. André and M. D. Lukin, Phys. Rev. Lett. **89**, 143602 (2002).
[24] M. Bajcsy, A. S. Zibrov, and M. D. Lukin, Nature **426**, 638 (2003).
[25] F. E. Zimmer, J. Otterbach, R. G. Unanyan, B. W. Shore, and M. Fleischhauer, Phys. Rev. A **77**, 063823 (2008).
[26] L.-M. Duan, M. D. Lukin, J. I. Cirac, and P. Zoller, Nature **414**, 413 (2001).
[27] N. Sangouard, C. Simon, H. de Riedmatten, and N. Gisin, Rev. Mod. Phys. **83**, 33 (2011).
[28] I. Iakoupov, J. R. Ott, D. E. Chang, and A. S. Sørensen, arXiv:1608.09016.
[29] See Supplemental Material for further details.
[30] S. Das, A. Grankin, I. Iakoupov, E. Brion, J. Borregaard, R. Boddeda, I. Usmani, A. Ourjoumtsev, P. Grangier, and A. S. Sørensen, Phys. Rev. A **93**, 040303 (2016).
[31] A. V. Gorshkov, A. André, M. D. Lukin, and A. S. Sørensen, Phys. Rev. A **76**, 033805 (2007).
[32] I. H. Deutsch, R. J. C. Spreeuw, S. L. Rolston, and W. D. Phillips, Phys. Rev. A **52**, 1394 (1995).
[33] L.-M. Duan, B. Wang, and H. J. Kimble, Phys. Rev. A **72**, 032333 (2005).
[34] J. Borregaard, P. Kómár, E. M. Kessler, A. S. Sørensen, and M. D. Lukin, Phys. Rev. Lett. **114**, 110502 (2015).
[35] J. Borregaard, P. Kómár, E. M. Kessler, M. D. Lukin, and A. S. Sørensen, Phys. Rev. A **92**, 012307 (2015).

Supplemental Material for "Controlled-phase gate for photons based on stationary light"

1. DUAL-V SCHEME

In this section, we list the differences of the dual-V scheme [S1] (Fig. 2(b) of the main article) from the Λ-type scheme (Fig. 2(a) of the main article), which was the focus of the discussion in the main article.

- There are two excited states $|b_\pm\rangle$ instead of only one. There are also two excited states $|e_\pm\rangle$ coupled to the state $|d\rangle$, instead of only one.
- The two classical drives have different polarizations, σ_+ and σ_-, and are therefore two independent running waves $\Omega_\pm(z) = \Omega_0 e^{\pm ik_0 z}$ instead of forming a standing wave. The quantum probe fields (single photon) and can also have two different polarizations. The operators for right-moving and left-moving fields with σ_+ polarization is $\hat{\mathcal{E}}_{\sigma_+,\pm}$, where "+" in the subscript is for the right-moving field and "−" is for the left-moving field. Similarly, $\hat{\mathcal{E}}_{\sigma_-,\pm}$ are the operators for the σ_- fields. The σ_+ fields only couple to the transitions $|a\rangle \leftrightarrow |b_+\rangle$ and $|d\rangle \leftrightarrow |e_+\rangle$, while the σ_- fields only couple to the transitions $|a\rangle \leftrightarrow |b_-\rangle$ and $|d\rangle \leftrightarrow |e_-\rangle$.
- The decay rate $\Gamma_{1\mathrm{D}}$ is from each of the states $|b_\pm\rangle$ (assumed equal).
- Two-mode transfer matrices are required to describe the scattering (more details in Sec. 3 below).
- Under EIT storage, we assume that only one of the classical drives is switched on, so that one of the excited states is decoupled from the dynamics. Hence, in this case, the dual-V scheme is completely equivalent to the Λ-type scheme. After storing a photon into state $|c\rangle$ and transferring it to state $|d\rangle$ by a π-pulse, for the dual-V scheme, the atom behaves as an effective V-type atom with two excited states $|e_\pm\rangle$, instead of a two-level atom.
- It is in principle possible to store the photon such that it is incident only from one side instead of symmetrically from both sides, as required for the Λ-type scheme.
- If one-sided storage is desired, a different setup can be used, where the photons are incident on the ensemble directly (without placing the ensemble inside a Sagnac interferometer). To convert between conditional reflection or transmission and conditional phase shift, a mirror behind the ensemble can be used. This setup may require less stabilization of path lengths than a Sagnac interferometer. The unconditional fidelity in this setup is found to be approximately the same, but the conditional fidelity has a worse scaling. The latter is because in Eqs. (3) and (4) of the main article, the terms linear in $(\tilde{z} - 1/2)$ do not cancel as in the symmetric case (also see the fidelity derivations in Sec. 6 below).

2. FIDELITY

Here, we state the expressions required for evaluating the Choi-Jamiolkowski fidelity and success probability accounting for non-zero bandwidth of the scattered photon B. We will also discuss, how the unconditional and conditional fidelities are related to figures of merit for quantum repeaters. A more detailed discussion can be found in Refs. [S2, S3].

The ideal evolution of the controlled-phase gate is defined by its action on the computation basis states

$$|00\rangle_{\mathrm{in}} \to |00\rangle_{\mathrm{out}}, \tag{S11}$$
$$|01\rangle_{\mathrm{in}} \to |01\rangle_{\mathrm{out}}, \tag{S12}$$
$$|10\rangle_{\mathrm{in}} \to |10\rangle_{\mathrm{out}}, \tag{S13}$$
$$|11\rangle_{\mathrm{in}} \to -|11\rangle_{\mathrm{out}}. \tag{S14}$$

To calculate the Choi-Jamiolkowski fidelity, we have to define the input basis states ($|jj'\rangle_{\mathrm{in}}$ for $j, j' \in \{0, 1\}$) and their ideal evolution into the output states ($|jj'\rangle_{\mathrm{out}}$). Since photon A is stored and retrieved, while photon B is scattered, it is most natural to describe the former as a temporal wave packet and the latter through a frequency distribution over δ_B, where $\delta_B = \Delta - \Delta_{\mathrm{c}}$ (see Figs. 2(a) and 2(b) of the main article) is the two-photon detuning. The ideal evolution is defined such that the output frequency distribution of photon B is equal to the input frequency

distribution, while the output wave packet of photon A is set to be the one obtained after storage and retrieval in the absence of scattering. In terms of the storage and retrieval kernels, $K_{\mathrm{s},j}(t_A)$ and $K_{\mathrm{r},j}(t_A)$ respectively (discussed in Sec. 5 below), the output wave packet of photon A is

$$\phi_{A,\mathrm{out},0}(t_A) = \sum_j \int K_{\mathrm{r},j}(t_A) K_{\mathrm{s},j}(t'_A) \phi_{A,\mathrm{in}}(t'_A)\,\mathrm{d}t'_A, \tag{S15}$$

where $\phi_{A,\mathrm{in}}$ is the input wave packet. We define $\phi_{A,\mathrm{out},0}$ to be unnormalized, and the absolute square of its norm $\int |\phi_{A,\mathrm{out},0}(t_A)|^2\,\mathrm{d}t_A = \eta_{\mathrm{EIT}}$ is the EIT storage and retrieval efficiency, which is, in general, less than unity due to imperfections. When defining the output basis states ($|jj'\rangle_{\mathrm{out}}$), we ensure that they are normalized by dividing them by $\sqrt{\eta_{\mathrm{EIT}}}$. In the numerical calculations, we use the discrete definition (S15) of $\phi_{A,\mathrm{out},0}$ (and similar one for $\phi_{A,\mathrm{out},1}$ below) instead of the continuum version that was stated in the main article for simplicity. The choices of $\phi_{A,\mathrm{out},0}$ and ϕ_B above are natural, but there may exist more optimal choices, which give better fidelities.

For the real physical evolution, we also need to calculate the output wave packet for photon A, when photon B was scattered from the ensemble. In this case, we have

$$\phi_{A,\mathrm{out},1}(t_A, \delta_B) = \sum_j \int K_{\mathrm{r},j}(t_A) R_{1,j}(\delta_B) K_{\mathrm{s},j}(t'_A) \phi_{A,\mathrm{in}}(t'_A)\,\mathrm{d}t'_A. \tag{S16}$$

Defining $\phi_{A,\mathrm{out},1}$ is necessary, because the reflection coefficient of the ensemble with a stored photon depends on the position of the atom, in which the photon was stored. The Choi-Jamiolkowski fidelity is computed by assuming a particular entangled state as the input and applying both the ideal and real evolution to it [S2–S4]. The fidelity between the output states is then the Choi-Jamiolkowski fidelity. It is given by

$$F_{\mathrm{CJ}} = \frac{\eta_{\mathrm{EIT}}}{16}\left| 2t_{\mathrm{b}} + \int R_0(\delta_B)|\phi_B(\delta_B)|^2\,\mathrm{d}\delta_B + \frac{1}{\eta_{\mathrm{EIT}}}\int\int \phi^*_{A,\mathrm{out},0}(t_A)\phi_{A,\mathrm{out},1}(t_A,\delta_B)|\phi_B(\delta_B)|^2\,\mathrm{d}t_A\,\mathrm{d}\delta_B \right|^2. \tag{S17}$$

If we neglect the bandwidth of photon B by setting ϕ_B to be a delta-function, $|\phi_B(\delta_B)|^2 = \delta(\delta_B - \delta_{\mathrm{res}})$, in the above expression, we obtain Eq. (5) of the main article.

The success probability for having two photons at the output is

$$P_{\mathrm{suc}} = \frac{\eta_{\mathrm{EIT}}}{4}\left(2|t_{\mathrm{b}}|^2 + \int |R_0(\delta_B)|^2|\phi_B(\delta_B)|^2\,\mathrm{d}\delta_B + \frac{1}{\eta_{\mathrm{EIT}}}\int\int |\phi_{A,\mathrm{out},1}(t_A,\delta_B)|^2|\phi_B(\delta_B)|^2\,\mathrm{d}t_A\,\mathrm{d}\delta_B \right). \tag{S18}$$

Setting $|\phi_B(\delta_B)|^2 = \delta(\delta_B - \delta_{\mathrm{res}})$, this reduces to Eq. (6) of the main article. The conditional Choi-Jamiolkowski fidelity is $F_{\mathrm{CJ,cond}} = F_{\mathrm{CJ}}/P_{\mathrm{suc}}$.

The abstract Choi-Jamiolkowski fidelity considered above can be related to more concrete figures of merit, such as entanglement swap fidelity and success probability in the setting of quantum repeaters. In Refs. [S2, S3] it is shown that the success probability of the entanglement swap operation is exactly the same as the success probability P_{suc} that we have defined above. Furthermore, since F_{CJ} measures the probability for the photons to be in the right modes with the right phase, whereas P_{suc} measures whether the photons are coming out, it holds that $F_{\mathrm{CJ}} \leq P_{\mathrm{suc}}$. The expressions for F_{CJ} stated in the main article thus give a lower bound for P_{suc}. For our particular implementation of the controlled-phase gate, most of the error in F_{CJ} is caused by photon loss, and hence we have $F_{\mathrm{CJ}} \approx P_{\mathrm{suc}}$. At the same time, $F_{\mathrm{CJ,cond}}$ is a lower bound and an approximation for the entanglement swap fidelity [S2, S3]. In Fig. S4, we illustrate the approximate equalities of F_{CJ} with P_{suc} and $F_{\mathrm{CJ,cond}}$ with the entanglement swap fidelity F_{swap}.

3. SCATTERING COEFFICIENTS FOR THE ENSEMBLE

3.1. Transfer matrix formalism

To find the scattering coefficients for an ensemble of Λ-type atoms, the single-mode transfer matrix formalism [S5] is sufficient. For the dual-V scheme, two different polarization modes of the electric field are coupled to the atoms, and hence a generalization to a two-mode transfer matrix formalism is required. The general multi-mode transfer matrix formalism is developed in Ref. [S6]. Here, we briefly summarize it before applying it to calculate the scattering coefficients of atomic ensembles.

In the multi-mode transfer matrix formalism, electric fields are described by vectors of $2n_{\mathrm{m}}$ elements, where n_{m} is the number of the different modes of the electric field. The fields propagating to the right and the fields propagating

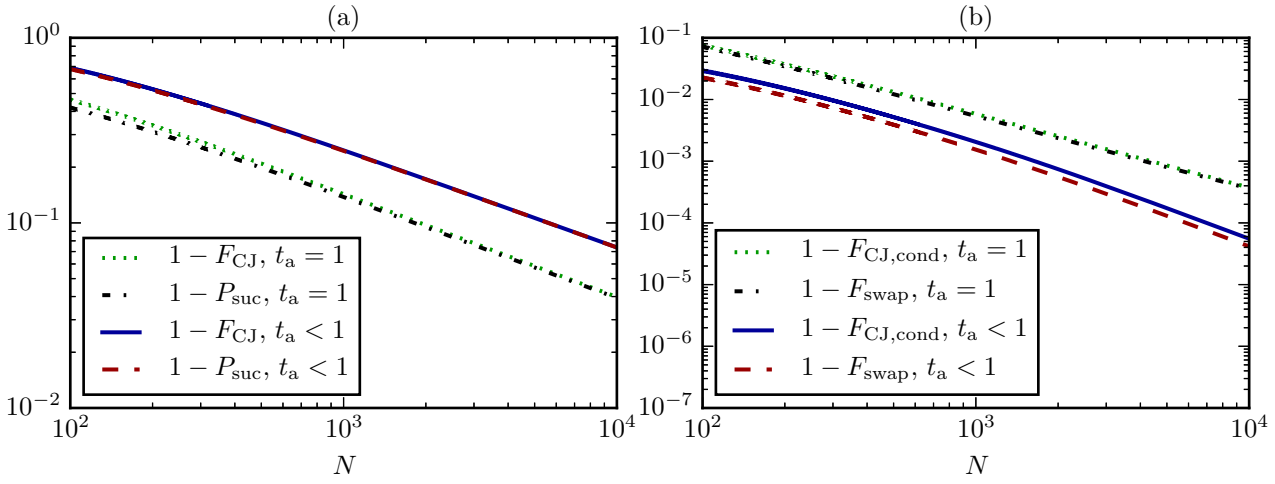

FIG. S4. (a) Comparison of the Choi-Jamiolkowski fidelity F_{CJ} for deterministic operation of the controlled-phase gate with the success probability P_{suc} for heralded operation of the gate. (b) Comparison of the conditional Choi-Jamiolkowski fidelity $F_{\mathrm{CJ,cond}}$ with the entanglement swap fidelity F_{swap} for heralded operation of the gate. Both for (a) and (b), dotted green and dash-dotted black curves are calculated with $t_{\mathrm{b}} = 1$, while the solid blue and dashed red curves are calculated with t_{b} chosen such that the entanglement swap fidelity F_{swap} is maximal. All quantities are plotted as functions of the number of atoms N with fixed $\Gamma_{1\mathrm{D}}/\Gamma = 0.5$. For storage and retrieval, we use the continuum theory described in Sec. 5.4.

to the left are treated as being distinct, hence there are n_{m} elements for each propagation direction. We can write the electric field vectors

$$\mathbf{E}(z) = \begin{pmatrix} \mathbf{E}_+(z) \\ \mathbf{E}_-(z) \end{pmatrix}, \tag{S19}$$

where $\mathbf{E}_+$ is the part of the electric field that propagates to the right (in the positive direction), $\mathbf{E}_-$ is the part of the electric field that propagates to the left (in the negative direction).

Atoms and free propagation between atoms are described by $2n_{\mathrm{m}} \times 2n_{\mathrm{m}}$ matrices, which relate the vectors of electric field at one position to vectors of electric field at a different position. In general, the transfer matrix for the whole ensemble is obtained by multiplying the transfer matrices for the atoms and free propagation. We use this approach for the dual-V atoms, for which we assume placement of the atoms, which is incommensurate with the wavelength of the classical drives (or even completely random). For the Λ-type scheme, the atoms are regularly placed with distance $\pi/(2k_0)$, as shown in Fig. S5. Hence, the ensemble consists of repeated unit cells, and one can instead exponentiate the transfer matrix for a single unit cell to find the transfer matrix for the whole ensemble. For Λ-type atoms described by 2×2 transfer matrices, closed-form expression can be obtained for the transfer matrix for the whole ensemble given in terms of the transfer matrix for the unit cell [S6]. If the transfer matrix for the unit cell is

$$T_{\mathrm{cell}} = \begin{pmatrix} T_{11} & T_{12} \\ T_{21} & T_{22} \end{pmatrix} \tag{S20}$$

then the transfer matrix for an ensemble of n such unit cells is

$$T_{\mathrm{cell}}^n = e^{in\theta A} = (\cos n\theta) I + i(\sin n\theta) A \tag{S21}$$

where I is the identity matrix,

$$A = \frac{1}{\sin\theta} \begin{pmatrix} i(T_{22} - T_{11})/2 & -iT_{12} \\ -iT_{21} & -i(T_{22} - T_{11})/2 \end{pmatrix}, \tag{S22}$$

and θ fulfills $\cos(\theta) = \mathrm{tr}(T_{\mathrm{cell}})/2 = (T_{11} + T_{22})/2$. Physically, θ is equal to the Bloch vector q multiplied by the length occupied by the unit cell. In the case of the Λ-type scheme with inter-atomic spacing $d = \lambda/4$ below, the unit cell has length $2d$ and hence we have $\theta = 2qd$.

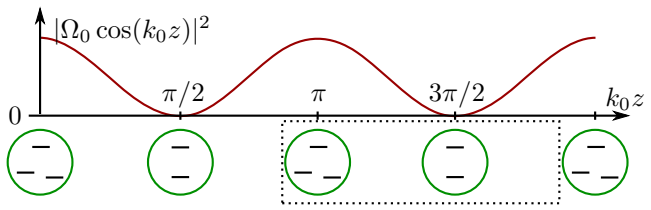

FIG. S5. Standing wave of the Rabi frequency of classical drive for the Λ-type scheme. The circles with 2 or 3 energy levels below the plot represent how the atoms will effectively behave in the different positions, i.e. either as two-level atoms on the nodes or as Λ-type atoms on the anti-nodes. The unit cell is shown by the dotted rectangle.

Once the transfer matrix for the ensemble T_e has been obtained, one needs to extract the scattering coefficients from it. The transfer matrix for the ensemble T_e fulfills the relation

$$\begin{pmatrix} \mathbf{E}_+(L^+) \\ \mathbf{E}_-(L^+) \end{pmatrix} = \begin{pmatrix} T_{\mathrm{e},11} & T_{\mathrm{e},12} \\ T_{\mathrm{e},21} & T_{\mathrm{e},22} \end{pmatrix} \begin{pmatrix} \mathbf{E}_+(0^-) \\ \mathbf{E}_-(0^-) \end{pmatrix}. \tag{S23}$$

For the dual-V atoms, the parts of the electric field vector $\mathbf{E}_\pm$ have two elements. To calculate the reflection coefficient of the ensemble, when the field is incident from the left, we assume input fields

$$\mathbf{E}_+(0^-) = \begin{pmatrix} 1 \\ 0 \end{pmatrix}, \quad \mathbf{E}_-(L^+) = \begin{pmatrix} 0 \\ 0 \end{pmatrix} \tag{S24}$$

(i.e. only a right-moving σ_+ field incident from the left). Then from Eq. (S23) we see that

$$\mathbf{E}_-(0^-) = -T_{\mathrm{e},22}^{-1} T_{\mathrm{e},12} \mathbf{E}_+(0^-), \tag{S25}$$

$$\mathbf{E}_+(L^+) = (T_{\mathrm{e},11} - T_{\mathrm{e},12} T_{\mathrm{e},22}^{-1} T_{\mathrm{e},21}) \mathbf{E}_+(0^-). \tag{S26}$$

As the transmission coefficient, we take the first (σ_+) element of $\mathbf{E}_+(L^+)$, and as the reflection coefficient, we take the second (σ_-) element of $\mathbf{E}_-(0^-)$. The reflection and transmission coefficients of the whole ensemble in the single-mode case simplify to $r_\mathrm{e} = -T_{\mathrm{e},21}/T_{\mathrm{e},22}$ and $t_\mathrm{e} = 1/T_{\mathrm{e},22}$ respectively.

The only thing left to describe in the general case, is how the matrix T_cell (and T_e if it is not simply equal to T_cell^n) is calculated. It is a product of the matrices $T_\mathrm{a}(\beta)$ describing scattering of the electric fields by the atoms and the matrices $T_\mathrm{f}(k_0 d)$ describing the free propagation of the electric fields. They are given by

$$T_\mathrm{a}(\beta) = \begin{pmatrix} I - \beta & -\beta \\ \beta & I + \beta \end{pmatrix}, \quad T_\mathrm{f}(k_0 d) = \begin{pmatrix} e^{ik_0 d} I & 0 \\ 0 & e^{-ik_0 d} I \end{pmatrix}, \tag{S27}$$

where I means the $n_\mathrm{m} \times n_\mathrm{m}$ identity matrix (a scalar equal to unity in the single-mode case), k_0 is the wave vector, and d is the propagation distance. Each matrix $T_\mathrm{a}(\beta)$ is given in terms a $n_\mathrm{m} \times n_\mathrm{m}$ matrix β, which will be defined for the specific cases of Λ-type and dual-V atoms considered below.

3.2. Reflection and transmission for the Λ-type scheme

3.2.1. Without a stored photon

Here, we derive the scattering coefficients r_0 and t_0 given by Eqs. (1) and (2) of the main article. For the Λ-type atoms, we use single-mode transfer matrices and hence the parameter β in Eq. (S27) is a scalar. We will consider a unit cell that consists of two atoms and two lengths of free propagation (see Fig. S5). One of the atoms is placed on the anti-node of the standing wave of the classical drive, and the other is placed on the node. The scattering from the former will be described by a parameter [S6]

$$\beta_3 = \frac{\Gamma_\mathrm{1D}\delta}{(\Gamma' - 2i\Delta)\delta + 2i|\Omega_0|^2}, \tag{S28}$$

while the scattering for the latter (an effective two-level atom) is described by a parameter

$$\beta_2 = \frac{\Gamma_{1D}}{\Gamma' - 2i\Delta}. \tag{S29}$$

The transfer matrix for the unit cell is

$$T_{\text{cell}} = T_{\text{f}}(\pi/2)T_{\text{a}}(\beta_2)T_{\text{f}}(\pi/2)T_{\text{a}}(\beta_3). \tag{S30}$$

Carrying out the above matrix multiplications results in

$$T_{\text{cell}} = \begin{pmatrix} -(1-\beta_2)(1-\beta_3) - \beta_2\beta_3 & \beta_3(1-\beta_2) - \beta_2(1+\beta_3) \\ \beta_2(1-\beta_3) - \beta_3(1+\beta_2) & -\beta_2\beta_3 - (1+\beta_2)(1+\beta_3) \end{pmatrix}. \tag{S31}$$

From Eq. (S21), we then have

$$T_{\text{e}} = T_{\text{cell}}^n = \cos(n\theta)\begin{pmatrix} 1 & 0 \\ 0 & 1 \end{pmatrix} + \frac{\sin(n\theta)}{\sin(\theta)}\begin{pmatrix} \beta_2+\beta_3 & -\beta_2+\beta_3-2\beta_2\beta_3 \\ \beta_2-\beta_3-2\beta_2\beta_3 & -\beta_2-\beta_3 \end{pmatrix} \tag{S32}$$

with θ given by $\cos(\theta) = \text{tr}(T_{\text{cell}})/2 = -1 - 2\beta_2\beta_3$. From this matrix, we obtain the reflection and transmission coefficients

$$r_0 = -\frac{T_{\text{e},21}}{T_{\text{e},22}} = \frac{-\beta_2+\beta_3+2\beta_2\beta_3}{\frac{\cos(n\theta)}{\sin(n\theta)}\sin(\theta) - (\beta_2+\beta_3)}, \tag{S33}$$

$$t_0 = \frac{1}{T_{\text{e},22}} = \frac{1}{\cos(n\theta) - \frac{\sin(n\theta)}{\sin(\theta)}(\beta_2+\beta_3)}. \tag{S34}$$

The minima of r_0 and maxima of t_0 (see Fig. 1 of the main article) occur when $\sin(n\theta)$ in Eq. (S21) is approximately equal to zero. However, exact equality is never satisfied, since θ is complex (a consequence of $\Gamma' > 0$). In the regime, where losses are small ($\text{Im}[\text{tr}(T_{\text{cell}})] \ll 1$), the approximate resonance condition is

$$\sin\big(n\arccos(\text{Re}[\text{tr}(T_{\text{cell}})]/2)\big) = 0. \tag{S35}$$

In the coefficients (S33) and (S34) we can approximate

$$\theta = \arccos(\text{tr}(T_{\text{cell}})/2) \approx \arccos(\text{Re}[\text{tr}(T_{\text{cell}})]/2) - \frac{i\,\text{Im}[\text{tr}(T_{\text{cell}})]/2}{\sqrt{(1-\text{Re}[\text{tr}(T_{\text{cell}})]/2)(1+\text{Re}[\text{tr}(T_{\text{cell}})]/2)}}. \tag{S36}$$

From Eq. (S35) we have

$$n\arccos(\text{Re}[\text{tr}(T_{\text{cell}})]/2) = \pi k \tag{S37}$$

for some integer k. Since the are interested in the first reflection minimum closest to $\delta = 0$, we choose $k = n-1$. For large n, we have

$$\text{Re}[\text{tr}(T_{\text{cell}})]/2 = \cos(\pi(n-1)/n) \approx -1 + \pi^2/(2n^2). \tag{S38}$$

Hence, Eq. (S36) can be approximated as

$$\theta \approx \pi(n-1)/n - in\,\text{Im}[\text{tr}(T_{\text{cell}})]/(2\pi), \tag{S39}$$

and we also obtain the approximate expressions:

$$\sin(n\theta) \approx (-1)^{n-1}\left(-in^2\,\text{Im}[\text{tr}(T_{\text{cell}})]/(2\pi)\right), \tag{S40}$$

$$\cos(n\theta) \approx (-1)^{n-1}, \tag{S41}$$

$$\sin(\theta) \approx \pi/n. \tag{S42}$$

With these approximations and using the fact that $\mathrm{Im}[\mathrm{tr}(T_{\mathrm{cell}})] = -4\,\mathrm{Im}[\beta_2\beta_3]$, Eqs. (S33) and (S34) become

$$r_0 \approx \frac{-\beta_2+\beta_3+2\beta_2\beta_3}{-\frac{i\pi^2}{2n^3\,\mathrm{Im}[\beta_2\beta_3]}-\beta_2-\beta_3}, \tag{S43}$$

$$t_0 \approx \frac{(-1)^{n-1}}{1-\frac{2in^3\,\mathrm{Im}[\beta_2\beta_3]}{i\pi^2}(\beta_2+\beta_3)}. \tag{S44}$$

To determine the dominant terms in Eqs. (S43) and (S44), we write the approximate expressions for Eqs. (S28) and (S29) in the limit, where δ is small, and $|\Delta_{\mathrm{c}}|$ is big ($\Delta = \Delta_{\mathrm{c}} + \delta$). We thereby get

$$\beta_3 \approx -i\frac{\Gamma_{1\mathrm{D}}\delta}{2|\Omega_0|^2}, \tag{S45}$$

$$\beta_2 \approx i\frac{\Gamma_{1\mathrm{D}}}{2\Delta}+\frac{\Gamma_{1\mathrm{D}}\Gamma'}{4\Delta^2}. \tag{S46}$$

The second term on the right hand side of Eq. (S46) is included for the sole purpose of finding an approximation for $\mathrm{Im}[\beta_2\beta_3] \approx \mathrm{Re}[\beta_2]\,\mathrm{Im}[\beta_3]$. An expression for the detuning δ can be found using Eq. (S38). Expanding its left hand side in δ around 0 to second order results in

$$\frac{\Gamma_{1\mathrm{D}}^2}{2\Delta_{\mathrm{c}}|\Omega_0|^2}\delta-\frac{\Gamma_{1\mathrm{D}}^2(|\Omega_0|^2-\Delta_{\mathrm{c}}^2)}{2\Delta_{\mathrm{c}}^2|\Omega_0|^4}\delta^2+\frac{\pi^2}{2n^2}=0. \tag{S47}$$

Under the assumption that $\Delta_{\mathrm{c}} < 0$, we choose the solution, where $\delta > 0$:

$$\frac{\delta}{|\Omega_0|^2} = \frac{\Delta_{\mathrm{c}}\left(-\Gamma_{1\mathrm{D}}+\sqrt{\Gamma_{1\mathrm{D}}-4(\Delta_{\mathrm{c}}^2-|\Omega_0|^2)\pi^2/n^2}\right)}{2\Gamma_{1\mathrm{D}}(\Delta_{\mathrm{c}}^2-|\Omega_0|^2)} \tag{S48}$$

Expanding this around the limit of large n we find

$$\frac{\delta}{|\Omega_0|^2} \approx -\frac{\Delta_{\mathrm{c}}\pi^2}{\Gamma_{1\mathrm{D}}^2n^2}-\frac{\Delta_{\mathrm{c}}^3\pi^4}{\Gamma_{1\mathrm{D}}^4n^4}+\frac{\Delta_{\mathrm{c}}|\Omega_0|^2\pi^4}{\Gamma_{1\mathrm{D}}^4n^4}. \tag{S49}$$

The first term on the right hand side of Eq. (S49) could also be derived from the knowledge that the dispersion relation is approximately quadratic for small δ, i.e. $\delta \approx (1/2m)(qd)^2 = (1/2m)(\theta d/2)^2$ with the mass m given in Ref. [S6], but the other two terms result from higher order corrections to this approximation. When we calculate the fidelity F_{CJ} in Sec. 6 below, we find that it is maximal for a detuning

$$|\Delta_{\mathrm{c}}| \propto \Gamma_{1\mathrm{D}}n^{3/4}. \tag{S50}$$

If we insert this expression into (S49), we find that the first term on the right hand side is proportional to $n^{-5/4}$, and the second one is proportional to $n^{-7/4}$. Hence, the second one is smaller for large n and can be neglected. We keep the third term, since it depends on Ω_0 and will be important when discussing the bandwidth of the protocol.

Using only the first term in Eq. (S49) and inserting it into the first term of Eq. (S46), we find

$$\beta_2 \approx i\frac{\Gamma_{1\mathrm{D}}}{2\Delta_{\mathrm{c}}\left(1-(\pi^2|\Omega_0|^2)/(\Gamma_{1\mathrm{D}}^2n^2)\right)} \approx i\frac{\Gamma_{1\mathrm{D}}}{2\Delta_{\mathrm{c}}}+i\frac{|\Omega_0|^2\pi^2}{2\Delta_{\mathrm{c}}\Gamma_{1\mathrm{D}}n^2}. \tag{S51}$$

Upon inserting into the second term of Eq. (S46), we find

$$\mathrm{Re}[\beta_2] \approx \frac{\Gamma_{1\mathrm{D}}\Gamma'}{4\Delta_{\mathrm{c}}^2\left(1-(\pi^2|\Omega_0|^2)/(\Gamma_{1\mathrm{D}}^2n^2)\right)^2} \approx \frac{\Gamma_{1\mathrm{D}}\Gamma'}{4\Delta_{\mathrm{c}}^2}+\frac{|\Omega_0|^2\pi^2\Gamma'}{2\Delta_{\mathrm{c}}^2\Gamma_{1\mathrm{D}}n^2}. \tag{S52}$$

Using the first and the third terms of Eq. (S49) and inserting them into Eq. (S45), we find

$$\beta_3 \approx -i\frac{\Gamma_{1\mathrm{D}}}{2}\left(-\frac{\Delta_{\mathrm{c}}\pi^2}{\Gamma_{1\mathrm{D}}^2n^2}+\frac{\Delta_{\mathrm{c}}|\Omega_0|^2\pi^4}{\Gamma_{1\mathrm{D}}^4n^4}\right) \approx i\frac{\Delta_{\mathrm{c}}\pi^2}{2\Gamma_{1\mathrm{D}}n^2}-i\frac{\Delta_{\mathrm{c}}|\Omega_0|^2\pi^4}{2\Gamma_{1\mathrm{D}}^3n^4}. \tag{S53}$$

Combining Eqs. (S52) and (S53) and neglecting a term of order n^{-6} results in

$$\mathrm{Im}[\beta_2\beta_3] \approx \mathrm{Re}[\beta_2]\,\mathrm{Im}[\beta_3] \approx \frac{\pi^2\Gamma'}{8\Delta_\mathrm{c} n^2} + \frac{|\Omega_0|^2\pi^4\Gamma'}{8\Delta_\mathrm{c}\Gamma_\mathrm{1D}^2 n^4}. \tag{S54}$$

Invoking Eq. (S50) again and neglecting the Ω_0 dependent terms for a moment, we see that $\beta_2 \propto n^{-3/4}$, $\beta_3 \propto n^{-5/4}$ and $n^3\,\mathrm{Im}[\beta_2\beta_3] \propto n^{1/4}$. Hence, $\beta_3 \ll \beta_2$; $\beta_2, \beta_3 \ll (n^3\,\mathrm{Im}[\beta_2\beta_3])^{-1}$ and we can approximate Eqs. (S43) and (S44) by

$$r_0 \approx -i\frac{2n^3}{\pi^2}\beta_2\,\mathrm{Im}[\beta_2\beta_3] \approx \frac{\Gamma_\mathrm{1D}\Gamma' n}{8\Delta_\mathrm{c}^2} + \frac{|\Omega_0|^2\pi^2\Gamma'}{4\Delta_\mathrm{c}^2\Gamma_\mathrm{1D} n}, \tag{S55}$$

$$t_0 \approx (-1)^{n-1}\left(1 + i\frac{2n^3}{\pi^2}\beta_2\,\mathrm{Im}[\beta_2\beta_3]\right) \approx (-1)^{n-1}\left(1 - \frac{\Gamma_\mathrm{1D}\Gamma' n}{8\Delta_\mathrm{c}^2} - \frac{|\Omega_0|^2\pi^2\Gamma'}{4\Delta_\mathrm{c}^2\Gamma_\mathrm{1D} n}\right). \tag{S56}$$

Since the number of atoms is $N = 2n$, the above expressions correspond to Eqs. (1) and (2) of the main article, except for the removal of the overall phase factor $(-1)^{n-1}$ for the transmission coefficient t_0 (discussed in Sec. 4 below). In Fig. S6(a) we plot $|t_0|^2$ as a function of Ω_0 and show that the analytical expression in Eq. (S56) matches the full expression in Eq. (S34) evaluated at the resonance frequency.

To account for the non-zero bandwidth of the scattered photon, we also need the width of the resonance. After expanding the reflection coefficient r_0 around δ_res, we get

$$r_0(\delta) \approx (2/w^2)(\delta - \delta_\mathrm{res})^2 + r_0(\delta_\mathrm{res}), \tag{S57}$$

where $r_0(\delta_\mathrm{res})$ is given by Eq. (S55) and

$$w = \frac{32\sqrt{2}\Delta_\mathrm{c}^2|\Omega_0|^2\pi^2}{\Gamma_\mathrm{1D}^3 N^3}, \tag{S58}$$

is the width. Since we approximately have that $t_0 \approx 1 - r_0$, the width of the transmission resonance is w. In Fig. S6(b) we compare Eq. (S58) with the numerically computed width.

3.2.2. With a stored photon

Here, we derive the scattering coefficients r_1 and t_1 given by Eqs. (3) and (4) of the main article. The starting point is the assumption that the photon has been stored in a single atom that is placed at the anti-node of the standing wave of the classical drive (storing in an atom that is on the node will have a negligible change in the scattering properties, unless $\Gamma_\mathrm{1D}/\Gamma$ is close to unity). The storage of a photon in the atom transfers it from state $|a\rangle$ to state $|d\rangle$, such that it behaves like a resonant two-level atom (given by the $|d\rangle \leftrightarrow |e\rangle$ transition) that is described by the transfer matrix $T_\mathrm{a}(\beta_{2,de})$ with

$$\beta_{2,de} = \frac{\Gamma_\mathrm{1D}}{\Gamma'}. \tag{S59}$$

Hence, the transfer matrix for the unit cell containing the stored photon will be given by

$$T_\mathrm{cell,ph} = T_\mathrm{f}(\pi/2)T_\mathrm{a}(\beta_2)T_\mathrm{f}(\pi/2)T_\mathrm{a}(\beta_{2,de}), \tag{S60}$$

instead of Eq. (S30). If we assume that the photon is stored in the unit cell with index n_ph, the transfer matrix for the whole ensemble $T_{\mathrm{e},n_\mathrm{ph}}$ is given by

$$T_{\mathrm{e},n_\mathrm{ph}} = T_\mathrm{cell}^{n-n_\mathrm{ph}} T_\mathrm{cell,ph} T_\mathrm{cell}^{n_\mathrm{ph}-1}. \tag{S61}$$

From Eq. (S61) we can find the scattering coefficients using

$$r_{1,n_\mathrm{ph}} = -\frac{T_{\mathrm{e},n_\mathrm{ph},21}}{T_{\mathrm{e},n_\mathrm{ph},22}}, \tag{S62}$$

$$t_{1,n_\mathrm{ph}} = \frac{1}{T_{\mathrm{e},n_\mathrm{ph},22}}, \tag{S63}$$

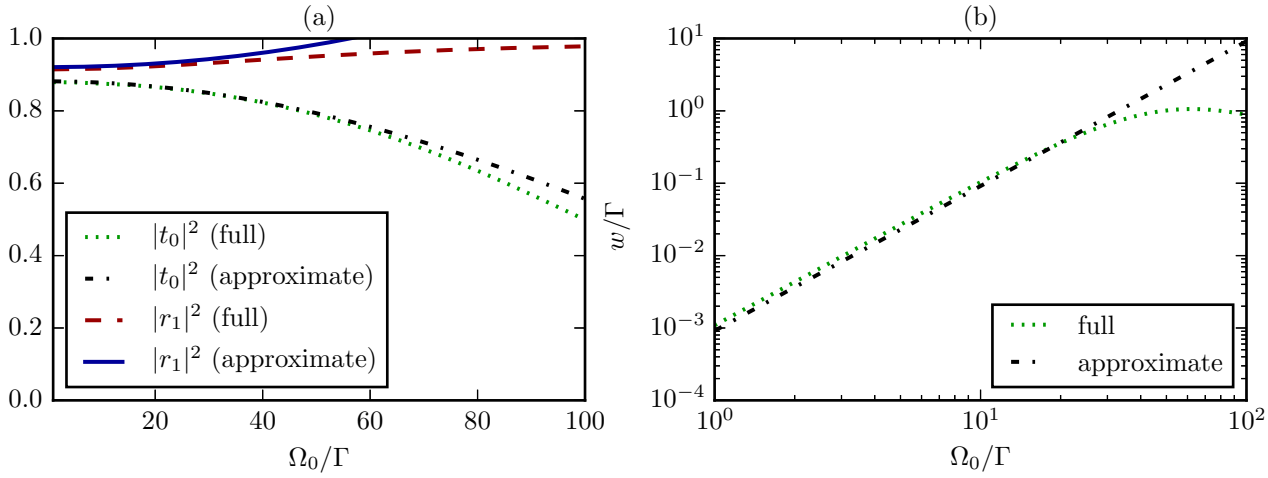

FIG. S6. (a) Reflectance with a stored photon $|r_1|^2$ and transmittance without a stored photon $|t_0|^2$ of an ensemble of Λ-type atoms plotted as functions of the Rabi frequency of the classical drive Ω_0 and evaluated at the transmission resonance closest to $\delta = 0$ (see Fig. 1 of the main article), i.e. at $\delta = \delta_{\rm res} \approx -4\Delta_{\rm c}\pi^2|\Omega_0|^2/(\Gamma_{\rm 1D}^2 N^2)$. Both t_0 and r_1 are calculated either directly from the transfer matrix with no approximations ("full"), which for t_0 is given by Eq. (S34), or from the approximate expressions in Eqs. (S56) and (S68) respectively ("approximate"). (b) The width of the transmission resonance calculated either from the full expression as $w = \mathrm{Re}\left[\sqrt{4/\partial_\delta^2 t_0(\delta)}\right]\Big|_{\delta=\delta_{\rm res}}$ or using the approximate expression (S58) (dash-dotted black). The parameters for both (a) and (b) are: number of atoms $N = 1000$, $\Gamma_{\rm 1D}/\Gamma = 0.5$, and $\Delta_{\rm c}/\Gamma = -16$. (The same as in Fig. 1 of the main article except for Ω_0, which is varied here.)

where $T_{{\rm e},n_{\rm ph},jj'}$ are the elements of the matrix $T_{{\rm e},n_{\rm ph}}$ similar to the definition (S23) of the elements of the matrix $T_{\rm e}$. For the numerical calculations, Eqs. (S62) and (S63) are used directly, and we set $R_{1,j} = -(r_{1,j} - t_{1,j})$ in Eq. (S16).

For the analytical calculations, we can find approximate expressions for the scattering coefficients, but the procedure is rather involved. We shall therefore restrict ourselves to a brief discussion of the main steps. We do several simplifications on the (very complicated) expressions resulting from Eqs. (S62) and (S63). We use the fact that $\beta_2\beta_3 = (-1-\cos(\theta))/2$ and the approximate expression $\theta \approx \pi(n-1)/n$. Also, while expanding the numerator and denominator around big n, we use that $\beta_2 \propto n^{-3/4}$ (a consequence of Eqs. (S29) and (S50)) to determine which terms can be neglected. Then we replace the index of the unit cell with the stored photon $n_{\rm ph}$ by $n\tilde{z}$, where $\tilde{z} = z/L$ is the rescaled position coordinate. After further approximating $1/n \approx 0$ and $n \pm 1 \approx n$, we get

$$r_1(\tilde{z}) = -\frac{\beta_{2,de}(\pi\cos(\pi\tilde{z}) - 2\beta_2 n\sin(\pi\tilde{z}))^2}{\sin^2(\pi\tilde{z})\left(\pi^2 - 4\beta_2^2\beta_{2,de}n^2\right) - 2\pi\beta_2^2\beta_{2,de}n\sin(2\pi\tilde{z}) + \pi^2(\beta_{2,de}+1)\cos^2(\pi\tilde{z})}, \tag{S64}$$

$$t_1(\tilde{z}) = \frac{(-1)^{n-1}\pi^2}{\sin^2(\pi\tilde{z})\left(\pi^2 - 4\beta_2^2\beta_{2,de}n^2\right) - 2\pi\beta_2^2\beta_{2,de}n\sin(2\pi\tilde{z}) + \pi^2(\beta_{2,de}+1)\cos^2(\pi\tilde{z})}. \tag{S65}$$

Next, we insert the expressions for β_2 and $\beta_{2,de}$ with the approximation $\Delta \approx \Delta_{\rm c}$, expand around $\tilde{z} = 1/2$, and use $|\Delta_{\rm c}| \propto \Gamma_{\rm 1D} n^{3/4}$ to identify which terms are dominant for $n \to \infty$. This results in

$$r_1(\tilde{z}) \approx 1 - \frac{\pi^2\Gamma'\Delta_{\rm c}^2}{\Gamma_{\rm 1D}^3 n^2} - \frac{2i\pi^2\Delta_{\rm c}}{\Gamma_{\rm 1D} n}\left(\tilde{z}-\frac{1}{2}\right) - \frac{\pi^4\Delta_{\rm c}^2(2\Gamma_{\rm 1D}+\Gamma')}{\Gamma_{\rm 1D}^3 n^2}\left(\tilde{z}-\frac{1}{2}\right)^2, \tag{S66}$$

$$t_1(\tilde{z}) \approx (-1)^{n-1}\left(\frac{\pi^2\Delta_{\rm c}^2\Gamma'}{\Gamma_{\rm 1D}^3 n^2} + \frac{\pi^4\Delta_{\rm c}^2\Gamma'}{\Gamma_{\rm 1D}^3 n^3}\left(\tilde{z}-\frac{1}{2}\right) + \frac{\pi^4\Delta_{\rm c}^2\Gamma'}{\Gamma_{\rm 1D}^3 n^2}\left(\tilde{z}-\frac{1}{2}\right)^2\right). \tag{S67}$$

We see that the resulting expressions do not depend on Ω_0. This is a consequence of approximating $\Delta \approx \Delta_{\rm c}$. If we use $\Delta = \Delta_{\rm c} + \delta$ together with Eq. (S49), we find corrections from the dependence on Ω_0. We only need the first term

in Eq. (S49) to find the lowest order correction due to Ω_0. At $\tilde{z} = 1/2$, and expanding around large n, we have

$$r_1 \approx 1 - \frac{\pi^2 \Delta_c^2 \Gamma'}{\Gamma_{1D}^3 n^2} + \frac{2\pi^4 \Delta_c^2 \Gamma' |\Omega_0|^2}{\Gamma_{1D}^5 n^4}, \tag{S68}$$

$$t_1 \approx (-1)^{n-1} \left(\frac{\Delta_c^2 \pi^2 \Gamma'}{\Gamma_{1D}^3 n^2} - \frac{2\pi^4 \Delta_c^2 \Gamma' |\Omega_0|^2}{\Gamma_{1D}^5 n^4} \right). \tag{S69}$$

In Fig. S6(a), we plot $|r_1|^2$ as a function of Ω_0 and show that the analytical expression in Eq. (S68) matches the full expression calculated using Eq. (S62) (evaluated at the resonance frequency) without doing any approximations. In Eq. (3) of the main article, we include all error terms of Eq. (S66) and also add the Ω_0 dependent error term from Eq. (S68). Likewise, in Eq. (4) of the main article, we include all error terms of Eq. (S67) and also add the Ω_0 dependent error term from Eq. (S69).

3.3. Reflection and transmission for the dual-V scheme

For the dual-V scheme, we need two-mode (4×4) transfer matrices to describe the σ_+ and σ_- polarized modes. The transfer matrices for the atoms in Eq. (S27) have the form $T_a(\beta_j)$ (j is the index of the atom), where [S6]

$$\beta_j = -(I + S_{j,r})^{-1} S_{j,r}, \tag{S70}$$

and

$$S_{j,r} = \begin{pmatrix} r_{j,++} & r_{j,-+} \\ r_{j,+-} & r_{j,--} \end{pmatrix}. \tag{S71}$$

In the above, we have used the same convention as in Eqs. (S24), i.e. that the first element of $E_\pm$ is the σ_+ component and the second element is the σ_- component. Hence, in Eq. (S71), r_{++} for example means the reflection coefficient, such that the incident σ_+ field is reflected also as a σ_+ field. Similarly for the other reflection coefficients.

If the atom is in state $|a\rangle$ (without a stored photon), the elements of $S_{j,r}$ are given by [S6]

$$r_{j,--} = r_{j,++} = -\frac{i(\Gamma_{1D}/2)\left(\Delta_\Gamma \delta - |\Omega_0|^2\right)}{\Delta_\Gamma^2 \delta - 2\Delta_\Gamma |\Omega_0|^2}, \tag{S72}$$

$$r_{j,-+} = -\frac{i(\Gamma_{1D}/2)|\Omega_0|^2}{\Delta_\Gamma^2 \delta - 2\Delta_\Gamma |\Omega_0|^2} e^{2ik_0 z_j}, \tag{S73}$$

$$r_{j,+-} = -\frac{i(\Gamma_{1D}/2)|\Omega_0|^2}{\Delta_\Gamma^2 \delta - 2\Delta_\Gamma |\Omega_0|^2} e^{-2ik_0 z_j}, \tag{S74}$$

where $\Delta_\Gamma = \Delta + i(\Gamma/2)$. If the atom is in state $|d\rangle$ (with a stored photon), it acts as a resonant V-type atoms, and hence the elements of $S_{j,r}$ are given by

$$r_{j,--} = r_{j,++} = -\frac{\Gamma_{1D}}{\Gamma}, \tag{S75}$$

$$r_{j,-+} = r_{j,+-} = 0. \tag{S76}$$

We will only calculate the reflection and transmission of ensembles of dual-V atoms numerically.

4. SAGNAC INTERFEROMETER AND ADJUSTMENT OF THE PHASES

Here, we calculate the result of scattering from the Sagnac interferometer shown in Fig. 2(d) of the main article. The sequential picture of the scattering is that the incident field on one of the ports is split by the 50:50 beam splitter, gets scattered by the ensemble, and then the transmitted and reflected parts will again interfere on the same beam splitter. Thus the matrix that relates the outputs to the inputs can be written

$$M_{\text{Sagnac}} = HSH, \tag{S77}$$

where the matrix H describes the beam splitter, and the matrix S describes the ensemble. We choose the phases of the beam splitter, such that it performs the Hadamard operation on the field, i.e.

$$H = \frac{1}{\sqrt{2}} \begin{pmatrix} 1 & 1 \\ 1 & -1 \end{pmatrix}, \tag{S78}$$

The ensemble can, in general, have different transmission and reflection coefficients depending on, whether the field is incident from the left or right. Therefore, we write

$$S = \begin{pmatrix} r_+ & t_+ \\ t_- & r_- \end{pmatrix}, \tag{S79}$$

where r_+ and t_+ are respectively the reflection and transmission coefficients when the field is incident from the left (propagating in the positive direction), and r_- and t_- are respectively the reflection and transmission coefficients when the field is incident from the right (propagating in the negative direction).

Multiplying the matrices, we get

$$M_{\text{Sagnac}} = \frac{1}{2} \begin{pmatrix} r_+ + t_+ + (r_- + t_-) & r_+ - t_+ - (r_- - t_-) \\ r_+ + t_+ - (r_- + t_-) & r_+ - t_+ + (r_- - t_-) \end{pmatrix}. \tag{S80}$$

For a standard (non-rotating) Sagnac interferometer where $r_+ = r_-$ and $t_+ = t_-$, we recover the well known result, that light always leaves the port in which it is incident [S7, S8]. Because the equality $r_+ = r_-$ need not be true, the off-diagonal entries of M_{Sagnac} are, in general, not zero and describe the leakage of the incident power to the other port of the Sagnac interferometer. However, due to the sequential operation of the gate, this leakage does not introduce any logic errors. Since scattering of photon B happens, while photon A is stored inside the ensemble, leakage of photon B into the rail that encodes state $|1\rangle_A$ (see Fig. 2(c) of the main article) is separated in time from the subsequent retrieval of photon A and hence can be either absorbed or rerouted along a different path.

Even though the off-diagonal entries of M_{Sagnac} are non-zero in general, they are strongly suppressed in the ideal limit, since e.g. both r_+ and r_- approach the same value (either 1 or 0 depending on, whether a photon was stored in the ensemble or not). As a concrete example, for the Λ-type scheme, we can use Eq. (S32) and find

$$r_{0+} = -\frac{T_{\text{e},21}}{T_{\text{e},22}} = \frac{-\beta_2 + \beta_3 + 2\beta_2\beta_3}{\frac{\cos(n\theta)}{\sin(n\theta)}\sin(\theta) - (\beta_2 + \beta_3)}, \tag{S81}$$

$$r_{0-} = \frac{T_{\text{e},12}}{T_{\text{e},22}} = \frac{-\beta_2 + \beta_3 - 2\beta_2\beta_3}{\frac{\cos(n\theta)}{\sin(n\theta)}\sin(\theta) - (\beta_2 + \beta_3)}, \tag{S82}$$

where r_{0+} is the same as r_0 (S33), and r_{0-} is the reflection coefficient where the field is incident from the right instead of the left. The difference between Eqs. (S81) and (S82) is only in the sign of the term $2\beta_2\beta_3$ in the numerator. As discussed above Eq. (S55), this term is much smaller than β_2 in the limit of large number of atoms and has therefore been neglected in Eq. (S55). Hence, Eq. (S55) can serve as an approximate expression for both r_{0+} and r_{0-}. We also note that it can be shown that the transmission coefficient for any 2×2 transfer matrix is independent of whether the field is incident from one side or the other (given by Eq. (S34) for t_0). However, we still account for the possible difference in the scattering coefficients in the numerical calculations (both for 2×2 and 4×4 transfer matrices) by defining the scattering coefficients R_0 and R_1 in Eqs. (S15) and (S16) as

$$R_0 = -(r_{0+} + r_{0-} - (t_{0+} + t_{0-}))/2, \tag{S83}$$

$$R_1 = -(r_{1+} + r_{1-} - (t_{1+} + t_{1-}))/2, \tag{S84}$$

where the scattering coefficients with "+" in the subscript assume incident photon from the left of the ensemble and the scattering coefficients with "−" in the subscript assume incident photon from the right of the ensemble.

We also need to discuss the choice of the phases in the interferometer. In Eq. (S77) there is an implicit assumption that the lengths of free propagation in the interferometer are chosen such that the distance from the beam splitter to either end of the ensemble is a multiple of the wavelength $\lambda = 2\pi/k_0$. Hence, the phase of free propagation is equal to unity for these parts. What we call "ensemble" may also contain some length of free propagation to the right of the ensemble to adjust the phases of its scattering coefficients.

To illustrate the necessity of phase adjustment, note that there is an overall phase factor $(-1)^{n-1}$ in Eqs. (S56), (S67), and (S69) compared with Eqs. (2) and (4) of the main article. If this phase factor is not removed, it will

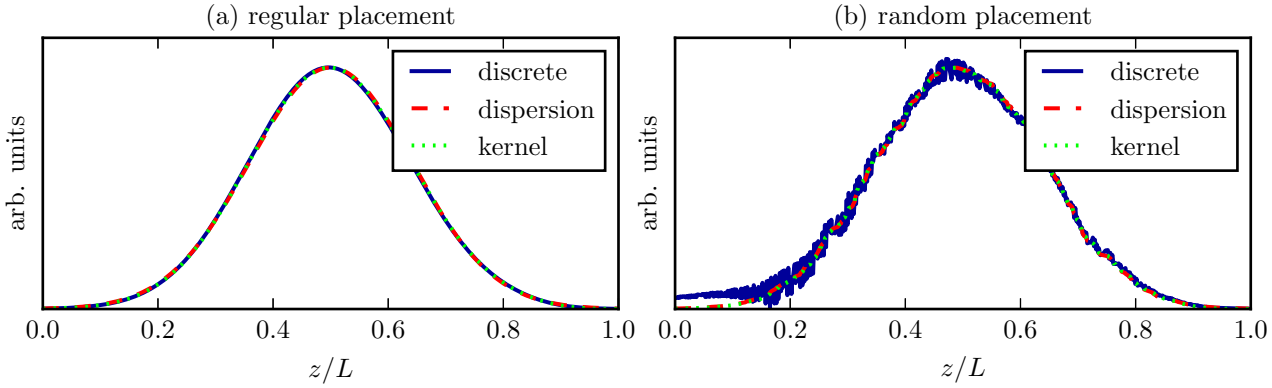

FIG. S7. The stored Gaussian spin wave computed using three different models for EIT storage: the dispersion relation of Sec. 5.2 ("dispersion"), the fully discrete theory of Sec. 5.3, and the storage kernel of Sec. 5.4 ("kernel"). Contrary to the fidelity calculations, here we assume EIT storage from one side (left) only to show the influence of random placement of the atoms more clearly. The common parameters for the two subplots are $\Gamma_{1D}/\Gamma = 0.5$, $N = 1000$, $\Omega_0/\Gamma = 1$, $\sigma/L = 0.1$ (width of the stored Gaussian spin wave). (a) Regularly placed atoms are assumed with inter-atomic distance $d = 0.266\pi/k_0$. All three curves are nearly indistinguishable from each other. (b) Randomly placed atoms, where the position of each atom is chosen from a uniform distribution over the whole ensemble. The average density is the same as in (a). The curve for the fully discrete storage is clearly distinct from the two others and exhibits rapid variation with position.

directly appear as a factor of R_0 (S83), when $r_{0\pm} \approx 0$ and $|t_{0\pm}| \approx 1$. Hence, the ideal value $R_0 = 1$ cannot be obtained even in the limit of many atoms. There are similar phase factor considerations for R_1 (S84) due the phase factor of the reflection coefficient r_{0-}, while r_{0+} is assumed to be at $z = 0$ and hence does not acquire phase factors with changing ensemble length. If the overall phase of the transmission coefficients is adjusted, the correct phase of R_0 and R_1 is obtained and the controlled-phase gate operation can approach the ideal limit as the number of the atoms is increased.

For the dual-V scheme, we can choose any inter-atomic spacing d, which is not a multiple of $\pi/(2k_0)$ (see Fig. S10 below). For this general case, we expect that instead of the overall phase factor $(-1)^{n-1}$, the transmission coefficients have the phase factor $\exp(ik_0L + \pi)$, which we likewise remove by adding a distance of free propagation d_{extra} to the right of the ensemble chosen such that $\exp(ik_0 d_{\text{extra}}) = \exp(-ik_0L - \pi)$. Multiplying this extra matrix of free propagation modifies the scattering coefficients according to

$$\begin{aligned} r_{0+} &\to r_{0+}, \\ r_{0-} &\to r_{0-} \exp(2ik_0 d_{\text{extra}}) \\ t_{0\pm} &\to t_{0\pm} \exp(ik_0 d_{\text{extra}}). \end{aligned} \tag{S85}$$

The physical interpretation of this mathematical result is that, since the free propagation was added on the right of the ensemble, then reflection for the field incident from the left (r_{0+}) is unaffected, while the reflection coefficient for fields incident from the right (r_{0-}) acquires twice the propagation phase. The transmission coefficients only acquire the propagation phase once.

The phase adjustments above effectively force the interferometer round trip length to be equal to an odd multiple of half wavelengths ($\exp(ik_0(L + d_{\text{extra}})) = -1$). Hence, the phase adjustment can be made independent of the number of atoms.

5. EIT STORAGE AND RETRIEVAL

5.1. Overview

We will model the EIT storage and retrieval process in three different ways:

1. Using the dispersion relation (see for instance Ref. [S9] and Sec. 5.2 below).

2. Using the fully discrete theory (see Ref. [S10] and Sec. 5.3 below).

3. Using the storage and retrieval kernels (see Ref. [S11] and Sec. 5.4 below).

We will consider the so-called adiabatic EIT storage [S11], where a single-photon wave packet is incident on the ensemble and is mapped onto a spin wave (a superposition of states, where a single atom is in state $|c\rangle$ and the rest are in state $|a\rangle$). We assume a constant Rabi frequency of the classical drive $\Omega(z,t) = \Omega_0$, but choosing a co-propagating classical drive with Rabi frequency $\Omega(z,t) = \Omega_0 e^{\pm ik_0 z}$ will only change the spatially-dependent phase factor of the stored spin wave. In the limit of high storage efficiency, the temporal profile of the photon and the spatial profile of the stored spin wave will approximately have the same form. E.g. if a photon with Gaussian temporal wave packet is stored, the resulting spin wave will have a Gaussian spatial profile. This is a consequence of the time-independent Rabi frequency of the classical drive and allows us to use the EIT dispersion relation to describe the storage and retrieval.

The EIT dispersion relation is used to gain intuition about the storage and retrieval process and also for the analytical calculations. In the numerical calculations of the fidelities and success probability, the atoms are always modeled as being discrete. Using the fully discrete EIT storage and retrieval model (Sec. 5.3) becomes very costly as the number of atoms increases. Therefore, to be able to calculate fidelities with a large number of atoms, we instead use the less computationally demanding storage and retrieval kernels derived in the continuum model and suitably discretized (Sec. 5.4). In Fig. S7, we show that the three models agree very well for the case of regularly placed ensembles with big optical depth $d_{\text{opt}} = 2N\Gamma_{1\text{D}}/\Gamma = 1000$. For randomly placed atoms, the fully discrete theory gives noticeably different results compared to using the discretized continuum theories (dispersion relation or storage kernel). Since we assume regular placement for the curves in Fig. 3 of the main article, the discretized storage and retrieval kernels are sufficient. We also verify this in Fig. S8 below for the Λ-type scheme, and the same conclusion holds for the dual-V scheme. In Fig. S11 below, where we show fidelities for randomly placed atoms, we only use the fully discrete model for storage and retrieval, even though it limits the maximal number of atoms that can be used in the calculations.

5.2. Using the dispersion relation

The adiabatic EIT storage and retrieval can be modeled in a particularly simple way if the influence of the interface between the atomic medium and vacuum is ignored. To use the EIT dispersion relation, we need to assume that the ensemble is of an infinite extent. However, to compute the the storage and retrieval efficiency, we need to assume propagation through a finite ensemble. In the calculations below, this is reflected in infinite bounds for the integration but a finite propagation length. The only processes that happen in this model is that the stored photon wave packet broadens in space as it propagates, and its norm decays due to spontaneous emission. The EIT storage and retrieval efficiency will then be the norm of the wave packet that has propagated for the full length of the ensemble L (with a stop at $L/2$ to allow for the second photon to be scattered off the ensemble).

The EIT dispersion relation is [S9]

$$\delta_k \approx v_{\text{g}}(k - k_0) + \frac{1}{2}\alpha(k - k_0)^2 \tag{S86}$$

with

$$v_{\text{g}} = \frac{2L|\Omega_0|^2}{N\Gamma_{1\text{D}}}, \quad \alpha = -i\frac{4L^2|\Omega_0|^2\Gamma'}{N^2\Gamma_{1\text{D}}^2}. \tag{S87}$$

In rescaled coordinates $\tilde{z} = z/L$ and wave vectors $\tilde{k} = kL$ the dispersion can be written

$$\delta_{\tilde{k}} \approx \tilde{v}_{\text{g}}(\tilde{k} - \tilde{k}_0) + \frac{1}{2}\tilde{\alpha}(\tilde{k} - \tilde{k}_0)^2 \tag{S88}$$

with

$$\tilde{v}_{\text{g}} = \frac{v_{\text{g}}}{L} = \frac{2|\Omega_0|^2}{N\Gamma_{1\text{D}}}, \quad \tilde{\alpha} = \frac{\alpha}{L^2} = -i\frac{4|\Omega_0|^2\Gamma'}{N^2\Gamma_{1\text{D}}^2}. \tag{S89}$$

We only consider incident photons where the temporal profile is Gaussian. When such a photon is mapped onto a stored excitation, this results in an approximately Gaussian spatial profile of the form

$$S(\tilde{z}) = \frac{1}{(2\pi\tilde{\sigma}^2)^{1/4}} \exp\left(-\frac{(\tilde{z} - \tilde{\mu})^2}{4\tilde{\sigma}^2}\right) e^{i\tilde{k}_0\tilde{z}}, \tag{S90}$$

where the rescaled quantities are $\tilde{\sigma} = \sigma/L$, $\tilde{\mu} = \mu/L$, $\tilde{k}_0 = \tilde{k}_0 L$. By Fourier transforming this wave function to get $\tilde{S}(\tilde{k})$, multiplying the Fourier transform by $\exp(-i\delta_{\tilde{k}}t)$ and Fourier transforming back we find

$$S(\tilde{z},t) = \frac{1}{(2\pi\tilde{\sigma}^2)^{1/4}}\sqrt{\frac{1}{1+i\tilde{\alpha}t/(2\tilde{\sigma}^2)}}\exp\left(-\frac{(\tilde{z}-\tilde{\mu}-\tilde{v}_{\mathrm{g}}t)^2}{4\tilde{\sigma}^2\left(1+i\tilde{\alpha}t/(2\tilde{\sigma}^2)\right)}\right)e^{i\tilde{k}_0\tilde{z}}. \tag{S91}$$

The norm squared of the wave packet at time $t \geq 0$ is given by

$$\mathcal{N}_S^2(t) = \int_{-\infty}^{\infty}|f(z,t)|^2 dz = \frac{1}{\sqrt{1+i\tilde{\alpha}t/(2\tilde{\sigma}^2)}}. \tag{S92}$$

The combined storage and retrieval efficiency is given by Eq. (S92) with $t = 1/\tilde{v}_{\mathrm{g}} = L/v_{\mathrm{g}}$, i.e. the time required to pass the whole ensemble. We thereby get

$$\eta_{\mathrm{EIT}} = \mathcal{N}_S^2(t = 1/\tilde{v}_{\mathrm{g}}) = \frac{1}{\sqrt{1+\frac{\Gamma'}{N\Gamma_{1\mathrm{D}}\tilde{\sigma}^2}}} \approx 1 - \frac{1}{2}\frac{\Gamma'}{N\Gamma_{1\mathrm{D}}\tilde{\sigma}^2}. \tag{S93}$$

5.3. Using the fully discrete theory

Using the intuition about EIT from Sec. 5.2, one can implement the numerical simulations of EIT storage and retrieval accounting for the discrete nature of atoms. This approach is very similar to the "electric field elimination" approach of Ref. [S10]. The main difference is that, since storage and retrieval of a single photon only requires calculating the dynamics in the atomic single-excitation manifold, we can eliminate the electric field directly in the Schrödinger picture instead of the Heisenberg picture like in Ref. [S10].

The electric field operator can be written $\hat{\mathcal{E}}(z) = \hat{\mathcal{E}}_+(z)e^{ik_0 z} + \hat{\mathcal{E}}_-(z)e^{ik_0 z}$, where $\hat{\mathcal{E}}_+$ and $\hat{\mathcal{E}}_-$ are the parts of the field that respectively propagate to the right (positive direction) and left (negative direction). The two parts are assumed to be completely separate fields, and their commutators are

$$[\hat{\mathcal{E}}_\alpha(z), \hat{\mathcal{E}}_\beta^\dagger(z')] = \delta_{\alpha\beta}\delta(z-z'), \tag{S94}$$

where $\alpha, \beta \in \{+,-\}$.

The Hamiltonian for the ensemble of Λ-type atoms coupled to the electric field is $\hat{H} = \hat{H}_{\mathrm{a}} + \hat{H}_{\mathrm{i}} + \hat{H}_{\mathrm{p}}$, representing the atomic, interaction and photonic Hamiltonian respectively. The three parts of the Hamiltonian are given by

$$\hat{H}_{\mathrm{a}} = -\hbar\sum_j\left[\left(\Delta_0 + i\frac{\Gamma'}{2}\right)\hat{\sigma}_{bb,j} + \delta_0\hat{\sigma}_{cc,j}\right], \tag{S95}$$

$$\hat{H}_{\mathrm{i}} = -\hbar\sum_j\left\{\left[\hat{\sigma}_{bc,j}\Omega_0 + \mathrm{H.c.}\right] + g\sqrt{2\pi}\left[\hat{\sigma}_{ba,j}\hat{\mathcal{E}}(z_j) + \mathrm{H.c.}\right]\right\}, \tag{S96}$$

$$\hat{H}_{\mathrm{p}} = -i\hbar c\int\left[\hat{\mathcal{E}}_+^\dagger(z)\frac{\partial\hat{\mathcal{E}}_+(z)}{\partial z} - \hat{\mathcal{E}}_-^\dagger(z)\frac{\partial\hat{\mathcal{E}}_-(z)}{\partial z}\right]\mathrm{d}z, \tag{S97}$$

where c is the group velocity in the waveguide. We assume that the detuning Δ_0 is always set to zero during storage and retrieval (this was also assumed in Sec. 5.2 above). However, if desired, off-resonant ($\Delta_0 \neq 0$) EIT storage and retrieval is also possible [S11], and hence we keep the Δ_0 term in the equations of motion below.

On the single-excitation manifold, the state can be written

$$|\psi(t)\rangle = \sum_j\left(P_j(t)\hat{\sigma}_{ba,j} + S_j(t)\hat{\sigma}_{ca,j}\right)|a\rangle^N|\mathrm{vac}\rangle \tag{S98}$$

$$+\left(\int\frac{\Phi_+(z,t)}{\sqrt{c}}\hat{\mathcal{E}}_+^\dagger(z)|\mathrm{vac}\rangle\,\mathrm{d}z + \int\frac{\Phi_-(z,t)}{\sqrt{c}}\hat{\mathcal{E}}_-^\dagger(z)|\mathrm{vac}\rangle\,\mathrm{d}z\right)|a\rangle^N. \tag{S99}$$

From the Schrödinger equation, we get the equations of motion for the atomic coefficients

$$\frac{\partial P_j}{\partial t} = i\left(\Delta_0 + i\frac{\Gamma'}{2}\right)P_j + i\Omega_0 S_j + i\sqrt{\frac{\Gamma_{1\mathrm{D}}}{2}}\left(\Phi_+(z_j,t)e^{ik_0 z_j} + \Phi_-(z_j,t)e^{-ik_0 z_j}\right), \tag{S100}$$

$$\frac{\partial S_j}{\partial t} = i\delta_0 S_j + i\Omega_0^* P_j, \tag{S101}$$

where $\Gamma_{1D} = 4\pi g^2/c$. For the electric field coefficients $\Phi_\pm$ we have the equations

$$\left(\frac{\partial}{\partial t} \pm c\frac{\partial}{\partial z}\right)\Phi_\pm(z,t) = ic\sqrt{\frac{\Gamma_{1D}}{2}}\sum_j \delta(z-z_j)P_j e^{\mp ik_0 z_j}. \tag{S102}$$

These equations can be formally solved, so that we obtain

$$\Phi_\pm(z,t) = \Phi_{\pm,\mathrm{in}}(z \mp ct) + i\sqrt{\frac{\Gamma_{1D}}{2}}\sum_j \theta\big(\pm(z-z_j)\big)\, P_j\left(t \mp \frac{z-z_j}{c}\right) e^{\mp ik_0 z_j}, \tag{S103}$$

where $\Phi_{\pm,\mathrm{in}}(z \pm ct)$ are the input fields, and θ is the Heaviside theta function. Inserting these solutions into Eq. (S100) and approximating $P_j\big(t - |z-z_j|/c\big) \approx P_j(t)$ [S10], we find

$$\frac{\partial P_j}{\partial t} = i\left(\Delta_0 + i\frac{\Gamma'}{2}\right)P_j + i\Omega_0 S_j + \frac{\Gamma_{1D}}{2}\sum_{j'} P_{j'} e^{ik_0|z_j - z_{j'}|} + i\sqrt{\frac{\Gamma_{1D}}{2}}\left(\Phi_{+,\mathrm{in}}(z_j - ct)e^{ik_0 z_j} + \Phi_{-,\mathrm{in}}(z_j + ct)e^{-ik_0 z_j}\right). \tag{S104}$$

The fidelity calculations in Sec. 2 above are formulated in terms of $\phi_{A,\mathrm{in}}(t)$ and $\phi_{A,\mathrm{out}}(t)$, which are respectively the input field to be stored and the retrieved output field. (There are two different output fields, $\phi_{A,\mathrm{out},0}(t)$ and $\phi_{A,\mathrm{out},1}(t)$, but for the discussion of storage and retrieval, the difference between them is not important.) We need to account for the beam splitter in the Sagnac interferometer. Hence, the relations between the fields in this section and Sec. 2 are

$$\Phi_{+,\mathrm{in}}(z_j - ct) = \frac{1}{\sqrt{2}}\phi_{A,\mathrm{in}}(t - z_j/c), \tag{S105}$$

$$\Phi_{-,\mathrm{in}}(z_j + ct) = \frac{1}{\sqrt{2}}\phi_{A,\mathrm{in}}(t - (L - z_j)/c), \tag{S106}$$

$$\phi_{A,\mathrm{out}}(t) = \frac{1}{\sqrt{2}}\left(\Phi_+(L,t) + \Phi_-(0,t)\right). \tag{S107}$$

Note that storage is done from two directions in order to ensure that no excitations are stored on atoms at the nodes of the standing wave of the classical drive applied during the scattering for the Λ-type scheme. The conditions for this may not necessarily be the same as the conditions derived for scattering from the Sagnac interferometer (see Sec. 4). If this is an issue, it can be compensated by adjusting the position of the atoms between storage and scattering, e.g., by adjusting the phases of the trapping lasers or of the classical drives. For the dual-V scheme, there is no phase requirement during storage and this is not a concern.

As the input wave function, we assume

$$\phi_{A,\mathrm{in}}(t) = \frac{1}{(2\pi\sigma_{\mathrm{in}}^2)^{1/4}}\exp\left(-\frac{(t-\mu_{\mathrm{in}}/c)^2}{4\sigma_{\mathrm{in}}^2}\right) \tag{S108}$$

where the width and central time

$$\sigma_{\mathrm{in}} = \sigma/\left(v_{\mathrm{g}}\sqrt{1 + i\alpha L/(4\sigma^2 v_{\mathrm{g}})}\right), \tag{S109}$$

$$\mu_{\mathrm{in}} = 4\sigma_{\mathrm{in}}, \tag{S110}$$

are defined in terms of the EIT group velocity (S87). The factor $\sqrt{1 + i\alpha L/(4\sigma^2 v_{\mathrm{g}})}$ (a real number, since α is imaginary) in the definition of σ_{in} is introduced to compensate for the spin wave becoming wider as it propagates inside the ensemble (see Eq. (S91)). This particular factor is chosen such that the stored Gaussian spin wave (centered at the position $L/2$) has width σ. In the end, since we optimize over σ, this adjustment has no effect on the final values of the numerically calculated fidelities and success probability. However, it ensures that the optimal σ in the numerical calculations is similar to the optimal value found by neglecting broadening of the spin wave under propagation.

In the fully discrete model, we do not explicitly calculate the storage and retrieval kernels that appear in Eqs. (S15) and (S16). Instead, we calculate the action of these kernels on respectively a specific $\phi_{A,\mathrm{in}}(t)$ or a spin wave given by the coefficients S_j. For storage, this amounts to numerically solving Eqs. (S101) and (S104) for a given

$\phi_{A,\mathrm{in}}(t)$ and the initial condition $P_j = S_j = 0$ at $t = 0$. We take the stored spin wave to be the coefficients S_j at $t = \mu_{\mathrm{in}}/c + L/(2v_{\mathrm{g}})$. This final time is the sum of the time for propagation through vacuum and (half of) the EIT medium. For retrieval, Eqs. (S101) and (S104) are solved with $\phi_{A,\mathrm{in}}(t) = 0$ under the initial conditions that at $t = 0$ the coefficients $S_j(t = 0)$ are set to the spin wave that is to be retrieved, and $P_j(t = 0) = 0$. At each time step, we calculate $\phi_{A,\mathrm{out}}(t)$ using Eq. (S103) with $P_j\big(t \mp (z - z_j)/c\big) \approx P_j(t)$ along with Eq. (S107). We assume that the retrieval happens until $t = L/v_{\mathrm{g}}$, i.e. the time that it takes for the EIT polaritons to move through the whole ensemble.

5.4. Using the storage and retrieval kernels

As an approximation to the fully discrete theory of Sec. 5.3, one can use the continuum theory of Ref. [S11]. The continuum approximation allows the derivation of explicit expressions for the linear maps (given in terms of integration with a particular kernel) describing storage and retrieval.

Before doing the continuum approximation, we first rewrite the Hamiltonian (S95) in terms of the collective operators

$$\hat{\sigma}_{\alpha\beta}(z) = \frac{1}{n_0}\sum_j \delta(z - z_j)\hat{\sigma}_{\alpha\beta,j}, \tag{S111}$$

where $\alpha, \beta \in \{a, b, c\}$, and $n_0 = N/L$ is the average density. These collective operators have the equal time commutation relation

$$[\hat{\sigma}_{\alpha\beta}(z), \hat{\sigma}_{\alpha'\beta'}(z')] = \frac{1}{n_0}\delta(z - z')(\delta_{\beta,\alpha'}\hat{\sigma}_{\alpha\beta'} - \delta_{\beta',\alpha}\hat{\sigma}_{\alpha'\beta}). \tag{S112}$$

Using the collective atomic operators, the Hamiltonian (S95) is

$$\hat{H}_{\mathrm{a}} = -\hbar n_0 \int \Big[\left(\Delta_0 + i\frac{\Gamma'}{2}\right)\hat{\sigma}_{bb}(z) + \delta_0\hat{\sigma}_{cc}(z)\Big]\,\mathrm{d}z \tag{S113}$$

$$\hat{H}_{\mathrm{i}} = -\hbar n_0 \int \left\{ \big[\hat{\sigma}_{bc}(z)\Omega_0 + \mathrm{H.c.}\big] + g\sqrt{2\pi}\left[\hat{\sigma}_{ba}(z)\hat{\mathcal{E}}(z) + \mathrm{H.c.}\right] \right\}\mathrm{d}z \tag{S114}$$

$$\hat{H}_{\mathrm{p}} = -i\hbar c \int \left[\hat{\mathcal{E}}_+^\dagger(z)\,\frac{\partial\hat{\mathcal{E}}_+(z)}{\partial z} - \hat{\mathcal{E}}_-^\dagger(z)\,\frac{\partial\hat{\mathcal{E}}_-(z)}{\partial z}\right]\mathrm{d}z. \tag{S115}$$

Instead of the state (S98), we use

$$|\psi(t)\rangle = \int \left(\frac{\sqrt{N}}{L}P(z,t)\hat{\sigma}_{ba}(z) + \frac{\sqrt{N}}{L}S(z,t)\hat{\sigma}_{ca}(z)\right)|a\rangle^N|\mathrm{vac}\rangle\,\mathrm{d}z \tag{S116}$$

$$+ \left(\int \frac{\Phi_+(z,t)}{\sqrt{c}}\hat{\mathcal{E}}_+^\dagger(z)|\mathrm{vac}\rangle\,\mathrm{d}z + \int \frac{\Phi_-(z,t)}{\sqrt{c}}\hat{\mathcal{E}}_-^\dagger(z)|\mathrm{vac}\rangle\,\mathrm{d}z\right)|a\rangle^N. \tag{S117}$$

Note that if, for example, the excitation is entirely in the metastable states at a time t, we have

$$1 = \langle\psi(t)|\psi(t)\rangle = \frac{N}{L^2}\int\int S^*(z,t)S(z',t)[\hat{\sigma}_{ab}(z), \hat{\sigma}_{ba}(z')]\,\mathrm{d}z = \frac{1}{L}\int\int |S(z,t)|^2\,\mathrm{d}z, \tag{S118}$$

where we have used the continuum approximation $\sum_j \delta(z - z_j) \approx n_0$ [S6] together with the low excitation approximation $\sigma_{aa,j} \approx 1$ to get $\sigma_{aa}(z) \approx 1$ and $\sigma_{bb} \approx 0$. Eq. (S118) also gives the normalization condition for S in the continuum model (and similarly for P).

The equations for the coefficients are

$$\left(\frac{\partial}{\partial t} \pm c\,\frac{\partial}{\partial z}\right)\Phi_\pm(z,t) = ic\sqrt{\frac{\Gamma_{1\mathrm{D}}N}{2}}\frac{1}{L}P(z,t), \tag{S119}$$

$$\frac{\partial}{\partial t}P(z,t) = i\left(\Delta_0 + i\frac{\Gamma'}{2}\right)P(z,t) + i\Omega_0 S(z,t) + i\sqrt{\frac{\Gamma_{1\mathrm{D}}N}{2}}\left(\Phi_+(z,t)e^{ik_0 z} + \Phi_-(z,t)e^{-ik_0 z}\right), \tag{S120}$$

$$\frac{\partial}{\partial t}S(z,t) = i\delta_0 S(z,t) + i\Omega_0^* P(z,t). \tag{S121}$$

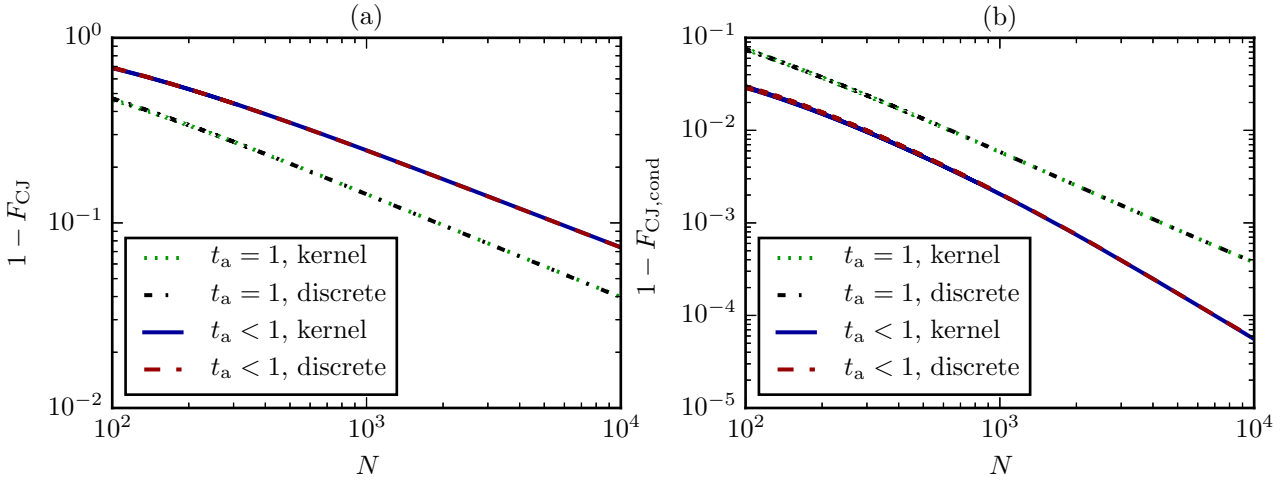

FIG. S8. Comparison of (a) unconditional and (b) conditional Choi-Jamiolkowski fidelities for the Λ-type scheme with different models used for EIT storage and retrieval plotted as functions of the number of atoms N with fixed $\Gamma_{1\mathrm{D}}/\Gamma = 0.5$. The "discrete" plots use the fully discrete theory of Sec. 5.3, and the "kernel" plots use the discretized storage and retrieval kernels derived in Sec. 5.4. In both cases, the optimal Δ_c and $\tilde{\sigma}$ (width of the stored Gaussian spin wave) are found by doing numerical optimization using the discretized storage and retrieval kernels, since the fully discrete model is much more computationally demanding.

As an extension to the theory of Ref. [S11], we want to consider an input field which is, in general, incident from both sides instead of only one. The approach that we use is to consider the parts of the single photon excitation incident from both sides as being stored separately from each other. When doing this we ignore the fact that the two parts have opposite spatial phases $e^{\pm ik_0 z}$, which interfere inside the ensemble to produce a spatially modulated spin wave with amplitude proportional to $\cos(k_0 z)$.

This spatial modulation of the stored spin wave is very important for the Λ-scheme, since the part of the excitation that is stored on the nodes of the standing wave of the classical drive does not significantly change the scattering properties of the ensemble (see Sec. 3.2.2). Expressed in terms of the notation introduced in the fidelity calculations (see Eq. (S16)) we have $R_{1,j}(\delta_B) \approx R_0(\delta_B)$ for odd j with atoms placed at positions $z_j = j\pi/(2k_0)$ $(0 \leq j \leq N-1)$, i.e. $k_0 z_j$ being an odd multiple of $\pi/2$. With the photon incident from both sides, we ensure that there is no amplitude on these atoms, since $S(z_j) \propto \cos(k_0 z_j) = 0$ for odd j. This is correctly reproduced by the fully discrete model of Sec. 5.3, since it always accounts for the phases of free propagation. On the other hand, due to the removal of the rapidly varying spatial phases in the continuum theory, this factor $\cos(k_0 z_j)$ is not present in the two separate parts of the stored spin wave. To compensate for this, we set $R_{1,j}(\delta_B) = R_{1,j-1}(\delta_B)$ for odd j. As we show in Fig. S8, this phenomenological adjustment of the reflection coefficient gives results that are essentially indistinguishable from the results produced by the fully discrete model of Sec. 5.3. For the dual-V scheme, no such adjustment of the reflection coefficients is needed neither in the continuum nor the discrete model, which also produce indistinguishable results.

The photons incident from the left and right couple to different components of the atomic coefficients, which can be written

$$P(z,t) = P_+(z,t)e^{ik_0 z} + P_-(z,t)e^{-ik_0 z}, \tag{S122}$$

$$S(z,t) = S_+(z,t)e^{ik_0 z} + S_-(z,t)e^{-ik_0 z}. \tag{S123}$$

After inserting these definitions into Eqs. (S119), (S120) and (S121) and separating the components, we get

$$\left(\frac{\partial}{\partial t} \pm c\frac{\partial}{\partial z}\right)\Phi_\pm(z,t) = ic\sqrt{\frac{\Gamma_{1\mathrm{D}}N}{2}}\frac{1}{L}P_\pm(z,t), \tag{S124}$$

$$\frac{\partial}{\partial t}P_\pm(z,t) = i\left(\Delta_0 + i\frac{\Gamma'}{2}\right)P_\pm(z,t) + i\Omega_0 S_\pm(z,t) + i\sqrt{\frac{\Gamma_{1\mathrm{D}}N}{2}}\Phi_\pm(z,t), \tag{S125}$$

$$\frac{\partial}{\partial t}S_\pm(z,t) = i\delta_0 S_\pm(z,t) + i\Omega_0^* P_\pm(z,t), \tag{S126}$$

To solve for Φ_+, P_+ and S_+, the approach in Ref. [S11] can be directly used. It consists of transforming into the coordinates $\tilde{z} = z/L$ and $\tilde{t} = t - z/c$, Laplace transforming in space, solving the algebraic equations of the Laplace transforms (under the adiabatic approximation $\frac{\partial}{\partial t}P_+ \approx 0$) and then Laplace transforming back. As a minor modification, we also transform back from the co-propagating time coordinate $\tilde{t} = t - z/c$ to the original t (by replacing all $\tilde{t}$ by t in the final expressions). Solving for Φ_-, P_- and S_- is simply a spatial reflection of the original problem around $\tilde{z} = 1/2$. We find that the stored spin wave is

$$S_+(\tilde{z}, t) = \int_0^{\tilde{t}} K_\mathrm{s}(\tilde{z}, t - t')\Phi_+(\tilde{z} = 0, t')\,\mathrm{d}t', \tag{S127}$$

$$S_-(\tilde{z}, t) = \int_0^{t} K_\mathrm{s}(1 - \tilde{z}, t - t')\Phi_-(\tilde{z} = 1, t')\,\mathrm{d}t', \tag{S128}$$

where the storage kernel (in the adiabatic approximation) is

$$K_\mathrm{s}(\tilde{z}, t) \approx -\frac{\sqrt{b}\Omega_0^* e^{i\delta_0 t}}{(\Gamma'/2) - i\Delta_0} I_0\left(2\frac{\sqrt{|\Omega_0|^2 t b\tilde{z}}}{(\Gamma'/2) - i\Delta_0}\right)\exp\left(-\frac{|\Omega_0|^2 t + b\tilde{z}}{(\Gamma'/2) - i\Delta_0}\right), \tag{S129}$$

written in terms of $b = (N\Gamma_{1\mathrm{D}})/2$ (related to the optical depth by $d_\mathrm{opt} = 4b/\Gamma$) and the modified Bessel function of the first kind I_0. The retrieved field is

$$\Phi_+(\tilde{z} = 1, t) = \int_0^1 K_\mathrm{r}(\tilde{z}, t)S_+(\tilde{z}, t = 0)\,\mathrm{d}\tilde{z}, \tag{S130}$$

$$\Phi_-(\tilde{z} = 0, t) = \int_0^1 K_\mathrm{r}(1 - \tilde{z}, t)S_-(\tilde{z}, t = 0)\,\mathrm{d}\tilde{z}, \tag{S131}$$

where the retrieval kernel is

$$K_\mathrm{r}(\tilde{z}, t) \approx -\frac{\sqrt{b}\Omega_0 e^{i\delta_0 t}}{(\Gamma'/2) - i\Delta_0} I_0\left(2\frac{\sqrt{|\Omega_0|^2 t b(1 - \tilde{z})}}{(\Gamma'/2) - i\Delta_0}\right)\exp\left(-\frac{|\Omega_0|^2 t + b(1 - \tilde{z})}{(\Gamma'/2) - i\Delta_0}\right). \tag{S132}$$

The stored spinwaves are chosen such that they are centered at $\tilde{z} = 1/2$ and become narrower in space for increasing optical depth (see the fidelity derivations in Sec. 6 below). The input and output photon wave functions are centered around times $t \propto L/v_\mathrm{g} = N\Gamma_{1\mathrm{D}}/(2|\Omega_0|^2) = b/|\Omega_0|^2$. Inserting these mean values into Eqs. (S129) and (S132), we see that the argument of I_0 becomes very big, since $\sqrt{|\Omega_0|^2 t b\tilde{z}} = \sqrt{|\Omega_0|^2 t b(1 - \tilde{z})} \propto b$ and $\Delta_0 = 0$. This allows us to use the asymptotic expansion $I_0(x) \approx \exp(x)/\sqrt{2\pi x}$, which is valid for $|x| \gg 1$ and $\arg(x) < \pi/2$. In this limit, the kernels become

$$K_\mathrm{s}(\tilde{z}, t) \approx -\frac{\sqrt{b}\Omega_0^* e^{i\delta t}}{2\sqrt{\pi}\sqrt{(\Gamma'/2) - i\Delta_0}} \frac{1}{\left(|\Omega_0|^2 t b\tilde{z}\right)^{1/4}} \exp\left(-\frac{\left(\sqrt{|\Omega_0|^2 t} - \sqrt{b\tilde{z}}\right)^2}{(\Gamma'/2) - i\Delta_0}\right), \tag{S133}$$

$$K_\mathrm{r}(\tilde{z}, t) \approx -\frac{\sqrt{b}\Omega_0 e^{i\delta t}}{2\sqrt{\pi}\sqrt{(\Gamma'/2) - i\Delta_0}} \frac{1}{\left(|\Omega_0|^2 t b(1 - \tilde{z})\right)^{1/4}} \exp\left(-\frac{\left(\sqrt{|\Omega_0|^2 t} - \sqrt{b(1 - \tilde{z})}\right)^2}{(\Gamma'/2) - i\Delta_0}\right). \tag{S134}$$

These formulas have a better numerical behavior compared to Eqs. (S129) and (S132), since one does not need to multiply the value of the I_0 (exponentially large) with an exponentially small factor. Hence, we always use Eqs. (S133) and (S134) in the numerical calculations.

The relations between the fields in this section and Sec. 2 are

$$\Phi_+(\tilde{z} = 0, t) = \frac{1}{\sqrt{2}}\phi_{A,\mathrm{in}}(t), \tag{S135}$$

$$\Phi_-(\tilde{z} = 1, t) = \frac{1}{\sqrt{2}}\phi_{A,\mathrm{in}}(t), \tag{S136}$$

$$\phi_{A,\mathrm{out}}(t) = \frac{1}{\sqrt{2}}\left(\Phi_+(\tilde{z} = 1, t) + \Phi_-(\tilde{z} = 0, t)\right). \tag{S137}$$

The results of this section assume that the atoms can be modeled as a continuum, but the scattering coefficients in Eq. (S16) are only given at the discrete atom positions. Hence, we need to sample the resulting continuum solutions at the discrete positions of the atoms. In the numerical calculations, the continuum solutions are always sampled as if the atoms were placed regularly independent of the actual placement. To justify regular sampling, we note that instead of the rescaled position coordinate $\tilde{z} = z/L$, one could use $\tilde{z} = \int_0^z (n_0(z')/N)\,\mathrm{d}z'$ [S11], where $n_0(z)$ is the local density of the atoms. For an average density $n_0 = N/L$, this rescaled coordinate is equivalent to $\tilde{z} = z/L$. For the local density $n_0(z) = \sum_j \delta(z - z_j)$, the rescaled position becomes $\tilde{z} = \sum_j \theta(z - z_j)/N$, where θ is the the Heaviside theta function. With the convention $\theta(0) = 0$, each z_j is transformed into $\tilde{z} = (j-1)/N$ regardless of the actual value of z_j. As shown in Fig. S7(b) for random placement of the atoms, even though the continuum solutions seem to be able to reproduce the results of the fully discrete theory to some degree, there are still significant differences, which we believe to be caused by reflection of parts of the propagating excitation due to disorder, which are not accounted for in the continuum theory. Hence, with randomly placed atoms, the fully discrete model is required.

Having in mind both the separation of the spin waves into two independent parts and the sampling of the continuum solutions at regular intervals, we can define the storage and retrieval kernels that will be used in Eqs. (S15) and (S16). We define the vector representing the spin wave to have $2N$ elements—for two separately stored spin waves that have fields incident either from the left or from the right as the input. Using the same storage time $\mu_{\mathrm{in}}/c + L/(2v_{\mathrm{g}})$ as for the discrete model in Sec. 5.3, the storage kernel is

$$K_{\mathrm{s},j}(t_A) = K_{\mathrm{s}}\big(\tilde{z} = j/N, t = \mu_{\mathrm{in}}/c + L/(2v_{\mathrm{g}}) - t_A\big)/\sqrt{N} \text{ for } 0 \le j \le N-1, \tag{S138}$$

$$K_{\mathrm{s},j}(t_A) = K_{\mathrm{s}}\big(\tilde{z} = 1 - (j-N)/N, t = \mu_{\mathrm{in}}/c + L/(2v_{\mathrm{g}}) - t_A\big)/\sqrt{N} \text{ for } N \le j \le 2N-1, \tag{S139}$$

where we have assumed that the coefficients corresponding to S_+ are stored in the part of the vector with indices $0 \le j \le N-1$, and the coefficients corresponding to S_- are stored in the part of the vector with $N \le j \le 2N-1$. The retrieval kernel is

$$K_{\mathrm{r},j}(t_A) = K_{\mathrm{r}}(\tilde{z} = j/N, t = t_A)/\sqrt{N} \text{ for } 0 \le j \le N-1, \tag{S140}$$

$$K_{\mathrm{r},j}(t_A) = K_{\mathrm{r}}(\tilde{z} = 1 - (j-N)/N, t = t_A)/\sqrt{N} \text{ for } N \le j \le 2N-1. \tag{S141}$$

As a consequence of having a spin wave vector with $2N$ elements, in Eq. (S16) we define $R_{1,j}(\delta_B) = R_{1,j-N}(\delta_B)$ for $N \le j \le 2N-1$.

6. ANALYTICAL FIDELITY OF THE GATE WITH Λ-TYPE ATOMS

Here, we derive Eqs. (7)–(10) of the main article. We also derive the bandwidth dependent correction to Eq. (7) of the main article, which is used in the discussion of the gate time.

From Eqs. (1)–(4) of the main article, we find the approximate reflection coefficients of the combined system of the atomic ensemble and the Sagnac interferometer. They are

$$R_0 = -(r_0 - t_0) \approx -\left(\frac{\Gamma_{1\mathrm{D}}\Gamma' N}{16\Delta_{\mathrm{c}}^2} - \left(1 - \frac{\Gamma_{1\mathrm{D}}\Gamma' N}{16\Delta_{\mathrm{c}}^2}\right)\right) = 1 - \frac{\Gamma_{1\mathrm{D}}\Gamma' N}{8\Delta_{\mathrm{c}}^2}, \tag{S142}$$

$$\begin{aligned} R_{1,\mathrm{s}}(\tilde{z}) &= \frac{1}{2}(R_1(\tilde{z}) + R_1(1-\tilde{z})) = -\frac{1}{2}\Big(r_1(\tilde{z}) + r_1(1-\tilde{z}) - \big(t_1(\tilde{z}) + t_1(1-\tilde{z})\big)\Big) \\ &\approx -\left(1 - \frac{8\pi^2\Delta_{\mathrm{c}}^2\Gamma'}{\Gamma_{1\mathrm{D}}^3 N^2} - \frac{8\pi^4\Delta_{\mathrm{c}}^2(\Gamma_{1\mathrm{D}} + \Gamma')}{\Gamma_{1\mathrm{D}}^3 N^2}\left(\tilde{z} - \frac{1}{2}\right)^2\right). \end{aligned} \tag{S143}$$

Note that in the symmetrized reflection coefficient $R_{1,\mathrm{s}}(\tilde{z})$, the linear terms proportional to $\pm(\tilde{z} - 1/2)$ (which are present in Eqs. (3) and (4) of the article) cancel each other. Using the expression for the spin wave given by Eq. (S90) with $\tilde{\mu} = 1/2$ we get

$$R_{1,1} \approx \int R_{1,\mathrm{s}}(\tilde{z})|S(\tilde{z})|^2\,\mathrm{d}\tilde{z} = -\left(1 - \frac{8\pi^2\Delta_{\mathrm{c}}^2\Gamma'}{\Gamma_{1\mathrm{D}}^3 N^2} - \frac{8\pi^4\Delta_{\mathrm{c}}^2(\Gamma_{1\mathrm{D}} + \Gamma')}{\Gamma_{1\mathrm{D}}^3 N^2}\tilde{\sigma}^2\right) \tag{S144}$$

Using Eq. (5) from the main article, an approximation for the unconditional CJ fidelity is

$$F_{\mathrm{CJ}} \approx 1 - \epsilon_{\mathrm{b}} - \frac{\Gamma_{1\mathrm{D}}\Gamma' N}{16\Delta_{\mathrm{c}}^2} - \frac{4\pi^2\Delta_{\mathrm{c}}^2\Gamma'}{\Gamma_{1\mathrm{D}}^3 N^2} - \frac{4\pi^4\Delta_{\mathrm{c}}^2(\Gamma_{1\mathrm{D}} + \Gamma')}{\Gamma_{1\mathrm{D}}^3 N^2}\tilde{\sigma}^2 - \frac{1}{2}\frac{\Gamma'}{N\Gamma_{1\mathrm{D}}}\frac{1}{\tilde{\sigma}^2}, \tag{S145}$$

where $\epsilon_\mathrm{b} = 1 - t_\mathrm{b}$, and all the error terms (including ϵ_b) are assumed to be small.

In principle, if we want to optimize the above expression, we should optimize with respect to Δ_c and $\tilde{\sigma}$ simultaneously (we do this in the numerical calculations). Here, we use an approximate optimization procedure, which ignores the fact that one of the error terms depends on the product of Δ_c and $\tilde{\sigma}$. As we will see, however, this error term is smaller than the error terms, which only depend on Δ_c for fixed $\Gamma_\mathrm{1D}/\Gamma$ and large N. Therefore, we first optimize F_CJ over Δ_c separately and then use the optimal value of Δ_c to optimize over $\tilde{\sigma}$. The optimal value of Δ_c is determined by the condition that the third and fourth error terms on the right hand side of Eq. (S145) are equal, i.e.

$$\frac{\Gamma_\mathrm{1D}\Gamma' N}{16\Delta_\mathrm{c}^2} = \frac{4\pi^2\Delta_\mathrm{c}^2\Gamma'}{\Gamma_\mathrm{1D}^3 N^2}. \tag{S146}$$

This results in

$$\Delta_\mathrm{c}^2 = \frac{\Gamma_\mathrm{1D}^2 N^{3/2}}{8\pi}. \tag{S147}$$

Inserting this value of Δ_c into Eq. (S145) we obtain

$$F_\mathrm{CJ} \approx 1 - \epsilon_\mathrm{b} - \frac{\pi\Gamma'}{\Gamma_\mathrm{1D}\sqrt{N}} - \frac{\pi^3(\Gamma_\mathrm{1D}+\Gamma')}{2\Gamma_\mathrm{1D}\sqrt{N}}\tilde{\sigma}^2 - \frac{1}{2}\frac{\Gamma'}{N\Gamma_\mathrm{1D}}\frac{1}{\tilde{\sigma}^2}. \tag{S148}$$

We use this expression to optimize over $\tilde{\sigma}$. The optimal $\tilde{\sigma}$ is obtained when

$$\frac{\pi^3(\Gamma_\mathrm{1D}+\Gamma')}{2\Gamma_\mathrm{1D}\sqrt{N}}\tilde{\sigma}^2 = \frac{1}{2}\frac{\Gamma'}{N\Gamma_\mathrm{1D}}\frac{1}{\tilde{\sigma}^2}. \tag{S149}$$

From this condition we get

$$\tilde{\sigma}^2 = \frac{1}{\pi^{3/2}N^{1/4}}\sqrt{\frac{\Gamma'}{\Gamma_\mathrm{1D}+\Gamma'}} \tag{S150}$$

and with this value of $\tilde{\sigma}$, Eq. (S148) becomes

$$F_\mathrm{CJ} \approx 1 - \epsilon_\mathrm{b} - \frac{\pi\Gamma'}{\Gamma_\mathrm{1D}\sqrt{N}} - \frac{\pi^{3/2}\sqrt{\Gamma_\mathrm{1D}+\Gamma'}\sqrt{\Gamma'}}{\Gamma_\mathrm{1D}N^{3/4}}. \tag{S151}$$

We see that for $N \to \infty$, the last term in this expression approaches zero faster than the second one. Hence, in Eqs. (7) and (9) of the main article we have omitted this term. The difference between Eq. (7) and Eq. (9) is whether we set respectively $\epsilon_\mathrm{b} = 0$ or $\epsilon_\mathrm{b} = 1 - R_0 = (\Gamma_\mathrm{1D}\Gamma' N)/(8\Delta_\mathrm{c}^2) = (\pi\Gamma')/(\Gamma_\mathrm{1D}\sqrt{N})$.

Next we calculate the conditional fidelity $F_\mathrm{CJ,cond}$. Since it is given by $F_\mathrm{CJ,cond} = F_\mathrm{CJ}/P_\mathrm{suc}$, the expansion of the ratio will contain higher order error terms than the expansion of the unconditional fidelity F_CJ. Hence, we need an expansion of F_CJ with more terms than in Eq. (S145). Including the second order terms and dividing out η_EIT (since it gets canceled in $F_\mathrm{CJ,cond}$), we get

$$\frac{F_\mathrm{CJ}}{\eta_\mathrm{EIT}} \approx 1 - \epsilon_\mathrm{b} - \frac{\Gamma_\mathrm{1D}\Gamma' N}{16\Delta_\mathrm{c}^2} - \frac{4\pi^2\Delta_\mathrm{c}^2\Gamma'}{\Gamma_\mathrm{1D}^3 N^2} - \frac{4\pi^4\Delta_\mathrm{c}^2(\Gamma_\mathrm{1D}+\Gamma')}{\Gamma_\mathrm{1D}^3 N^2}\tilde{\sigma}^2 \tag{S152}$$

$$+ \left(\frac{1}{2}\epsilon_\mathrm{b} + \frac{\Gamma_\mathrm{1D}\Gamma' N}{32\Delta_\mathrm{c}^2} + \frac{2\pi^2\Delta_\mathrm{c}^2\Gamma'}{\Gamma_\mathrm{1D}^3 N^2} + \frac{2\pi^4\Delta_\mathrm{c}^2(\Gamma_\mathrm{1D}+\Gamma')}{\Gamma_\mathrm{1D}^3 N^2}\tilde{\sigma}^2\right)^2 \tag{S153}$$

Using Eq. (6), we also get the success probability

$$\frac{P_\mathrm{suc}}{\eta_\mathrm{EIT}} = \frac{1}{4}\left(2(1-\epsilon_\mathrm{b})^2 + \left(1 - \frac{\Gamma_\mathrm{1D}\Gamma' N}{8\Delta_\mathrm{c}^2}\right)^2 + R_{1,2}\right), \tag{S154}$$

where

$$R_{1,2} \approx \int |R_{1,\mathrm{s}}(\tilde{z})|^2 |S(\tilde{z})|^2 \,\mathrm{d}\tilde{z} \tag{S155}$$

$$= 1 - \frac{16\pi^2\Delta_\mathrm{c}^2\Gamma'}{\Gamma_\mathrm{1D}^3 N^2} - \frac{16\pi^4\Delta_\mathrm{c}^2(\Gamma_\mathrm{1D}+\Gamma')}{\Gamma_\mathrm{1D}^3 N^2}\tilde{\sigma}^2 + \left(\frac{8\pi^2\Delta_\mathrm{c}^2\Gamma'}{\Gamma_\mathrm{1D}^3 N^2}\right)^2 + \left(\frac{8\pi^4\Delta_\mathrm{c}^2(\Gamma_\mathrm{1D}+\Gamma')}{\Gamma_\mathrm{1D}^3 N^2}\right)\left(3\tilde{\sigma}^4\right) \tag{S156}$$

$$+ 2\left(\frac{8\pi^2\Delta_\mathrm{c}^2\Gamma'}{\Gamma_\mathrm{1D}^3 N^2}\right)\left(\frac{8\pi^4\Delta_\mathrm{c}^2(\Gamma_\mathrm{1D}+\Gamma')}{\Gamma_\mathrm{1D}^3 N^2}\right)\tilde{\sigma}^2. \tag{S157}$$

Using the above expressions, the conditional fidelity can be written

$$F_{\mathrm{CJ,cond}} \approx 1 - \epsilon_{\mathrm{cond},1} - \epsilon_{\mathrm{cond},2}, \tag{S158}$$

where

$$\epsilon_{\mathrm{cond},1} = \frac{1}{4}\left(2\epsilon_{\mathrm{b}}^2 + \left(\frac{\Gamma_{1\mathrm{D}}\Gamma' N}{8\Delta_{\mathrm{c}}^2}\right)^2 + \left(\frac{8\pi^2\Delta_{\mathrm{c}}^2\Gamma'}{\Gamma_{1\mathrm{D}}^3 N^2}\right)^2\right) - \frac{1}{16}\left(2\epsilon_{\mathrm{b}} + \frac{\Gamma_{1\mathrm{D}}\Gamma' N}{8\Delta_{\mathrm{c}}^2} + \frac{8\pi^2\Delta_{\mathrm{c}}^2\Gamma'}{\Gamma_{1\mathrm{D}}^3 N^2}\right)^2, \tag{S159}$$

$$\epsilon_{\mathrm{cond},2} = \frac{44\pi^8\Delta_{\mathrm{c}}^4(\Gamma_{1\mathrm{D}}+\Gamma')^2}{\Gamma_{1\mathrm{D}}^6 N^4}\tilde{\sigma}^4. \tag{S160}$$

Using the Δ_{c} from Eq. (S147), we get

$$\epsilon_{\mathrm{cond},1} = \frac{1}{2}\left(\epsilon_{\mathrm{b}}^2 + \left(\frac{\pi\Gamma'}{\Gamma_{1\mathrm{D}}\sqrt{N}}\right)^2\right) - \frac{1}{4}\left(\epsilon_{\mathrm{b}} + \frac{\pi\Gamma'}{\Gamma_{1\mathrm{D}}\sqrt{N}}\right)^2, \tag{S161}$$

$$\epsilon_{\mathrm{cond},2} = \frac{11\pi^6(\Gamma_{1\mathrm{D}}+\Gamma')^2}{\Gamma_{1\mathrm{D}}^2 N}\tilde{\sigma}^4. \tag{S162}$$

If we choose $\epsilon_{\mathrm{b}} = 0$, $\epsilon_{\mathrm{cond},1}$ is the dominant error term with the value

$$\epsilon_{\mathrm{cond},1} = \frac{1}{4}\left(\frac{\pi\Gamma'}{\Gamma_{1\mathrm{D}}\sqrt{N}}\right)^2, \tag{S163}$$

in which case $\epsilon_{\mathrm{cond},2}$ can be neglected. If we choose $\epsilon_{\mathrm{b}} = (\pi\Gamma')/(\Gamma_{1\mathrm{D}}\sqrt{N})$, we get $\epsilon_{\mathrm{cond},1} = 0$, and we need to keep $\epsilon_{\mathrm{cond},2}$. The value of $\epsilon_{\mathrm{cond},2}$ depends on the width of the stored Gaussian $\tilde{\sigma}$. For simplicity, we use the value of $\tilde{\sigma}$ given by Eq. (S150), which makes the unconditional fidelity maximal. With this choice, the conditional fidelity is given by Eq. (10) of the main article. A comparison of the analytical formulas and the numerical results for F_{CJ} and $F_{\mathrm{CJ,cond}}$ is shown in Fig. S9.

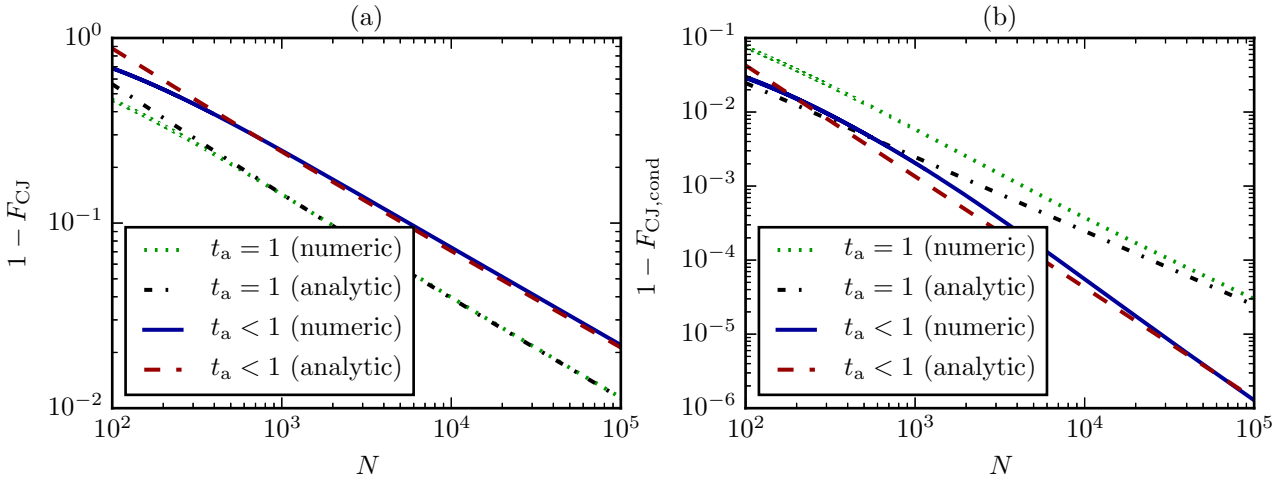

FIG. S9. Comparison of (a) unconditional and (b) conditional Choi-Jamiolkowski fidelities for the Λ-type scheme plotted as functions of the number of atoms N with fixed $\Gamma_{1\mathrm{D}}/\Gamma = 0.5$. Dotted green curves are the numerically calculated fidelities with $t_{\mathrm{b}} = 1$. Dash-dotted black curves are the approximate analytical results given by Eq. (7) (unconditional) and Eq. (8) (conditional) of the main article. Solid blue curves are the numerically calculated fidelities with t_{b} chosen such that the entanglement swap fidelity (which is approximately equal to the conditional Choi-Jamiolkowski fidelity as shown in Fig. S4) is maximal. The dashed red curves are the approximate analytical results given by Eq. (9) (unconditional) and Eq. (10) (conditional) of the main article. For storage and retrieval in the numerical calculations, we use the discretized continuum theory described in Sec. 5.4.

Now we derive the correction to the unconditional fidelity due to non-zero bandwidth of the scattered photon B. The general expression for the fidelity is given by Eq. (S17). As discussed in the main article, we ignore the non-zero

bandwidth in the last term since the variation of r_1 and t_1 with frequency around the resonance detuning $\delta_{\rm res}$ is smaller than variation of r_0 and t_0. Hence, we approximate

$$\frac{1}{\eta_{\rm EIT}}\int\int \phi^*_{A,{\rm out},0}(t_A)\phi_{A,{\rm out},1}(t_A,\delta_B)|\phi_B(\delta_B)|^2\,{\rm d}t_A\,{\rm d}\delta_B \approx (1/\eta_{\rm EIT})\int \phi^*_{A,{\rm out},0}(t)\phi_{A,{\rm out},1}(t)\,{\rm d}t = R_{1,1} \tag{S164}$$

such that the expression for the fidelity becomes

$$F_{\rm CJ} = \frac{\eta_{\rm EIT}}{16}\left|2t_{\rm b} + \int R_0(\delta_B)|\phi_B(\delta_B)|^2\,{\rm d}\delta_B + R_{1,1}\right|^2. \tag{S165}$$

Using Eqs. (S57) and (S58) together with expressions $t_0 \approx 1-r_0$ and $R_0 = -(r_0 - t_0)$ and defining the spectral width of photon B by $\sigma_B = \int(\delta-\delta_{\rm res})^2|\phi_B(\delta_B)|^2\,{\rm d}\delta_B$, we get

$$\int R_0(\delta)|\phi_B(\delta_B)|^2\,{\rm d}\delta_B \approx R_0(\delta_{\rm res}) - (4/w^2)\sigma_B^2 \approx 1 - \frac{\Gamma_{\rm 1D}\Gamma' N}{8\Delta_{\rm c}^2} - \frac{\Gamma'|\Omega_0|^2\pi^2}{\Delta_{\rm c}^2\Gamma_{\rm 1D}N} - \frac{\Gamma_{\rm 1D}^6 N^6}{512\Delta_{\rm c}^4|\Omega_0|^4\pi^4}\sigma_B^2. \tag{S166}$$

Using the optimal $\Delta_{\rm c}$ from Eq. (S147), this becomes

$$\int R_0(\delta)|\phi_B(\delta_B)|^2\,{\rm d}\delta_B \approx 1 - \frac{\pi\Gamma'}{\Gamma_{\rm 1D}\sqrt{N}} - \frac{8\Gamma'|\Omega_0|^2\pi^3}{\Gamma_{\rm 1D}^3 N^{5/2}} - \frac{\Gamma_{\rm 1D}^2 N^3}{8|\Omega_0|^4\pi^2}\sigma_B^2. \tag{S167}$$

To minimize the sum of the two last error terms in this expression, we optimize over Ω_0 and get

$$\int R_0(\delta)|\phi_B(\delta_B)|^2\,{\rm d}\delta_B \approx 1 - \frac{\pi\Gamma'}{\Gamma_{\rm 1D}\sqrt{N}} - \frac{3\times 2^{1/3}\pi^{4/3}\Gamma'^{2/3}}{\Gamma_{\rm 1D}^{4/3}N^{2/3}}\sigma_B^{2/3} \tag{S168}$$

for the optimal

$$|\Omega_0|^2 = \frac{\Gamma_{\rm 1D}^{5/3}N^{11/6}\sigma_B^{2/3}}{2^{5/3}\pi^{5/3}\Gamma'^{1/3}}. \tag{S169}$$

Then the fidelity (S165) is

$$F_{\rm CJ} \approx 1 - \epsilon_{\rm b} - \frac{\pi\Gamma'}{\Gamma_{\rm 1D}\sqrt{N}} - \frac{\pi^{3/2}\sqrt{\Gamma_{\rm 1D}+\Gamma'}\sqrt{\Gamma'}}{\Gamma_{\rm 1D}N^{3/4}} - \frac{3\pi^{4/3}\Gamma'^{2/3}}{2^{2/3}\Gamma_{\rm 1D}^{4/3}N^{2/3}}\sigma_B^{2/3}, \tag{S170}$$

i.e. compared to Eq. (S151), there is an extra error term that depends on σ_B.

7. DEPENDENCE ON POSITIONS OF THE ATOMS

While the Λ-type scheme is highly sensitive to the exact placement of the atoms, the dual-V scheme is much less sensitive. To verify this, we numerically evaluate the gate performance for various placements of the atoms. First, we investigate the dependence for regularly placed dual-V atoms with different interatomic spacings d. In Fig. S10, we see that for $k_0 d$ different from multiples of $\pi/2$, both the conditional and unconditional fidelities are approximately constant.

Second, we consider randomly placed dual-V atoms. In Fig. S11, the fidelities with regular and random placement are seen to have qualitatively the same behavior, but the performance with random placement is slightly worse.

[S1] F. E. Zimmer, J. Otterbach, R. G. Unanyan, B. W. Shore, and M. Fleischhauer, Phys. Rev. A **77**, 063823 (2008).
[S2] S. Das, A. Grankin, I. Iakoupov, E. Brion, J. Borregaard, R. Boddeda, I. Usmani, A. Ourjoumtsev, P. Grangier, and A. S. Sørensen, arXiv:1506.04300.
[S3] I. Iakoupov and A. S. Sørensen, In preparation.
[S4] A. Gilchrist, N. K. Langford, and M. A. Nielsen, Phys. Rev. A **71**, 062310 (2005).
[S5] I. H. Deutsch, R. J. C. Spreeuw, S. L. Rolston, and W. D. Phillips, Phys. Rev. A **52**, 1394 (1995).
[S6] I. Iakoupov, J. R. Ott, D. E. Chang, and A. S. Sørensen, arXiv:1608.09016.

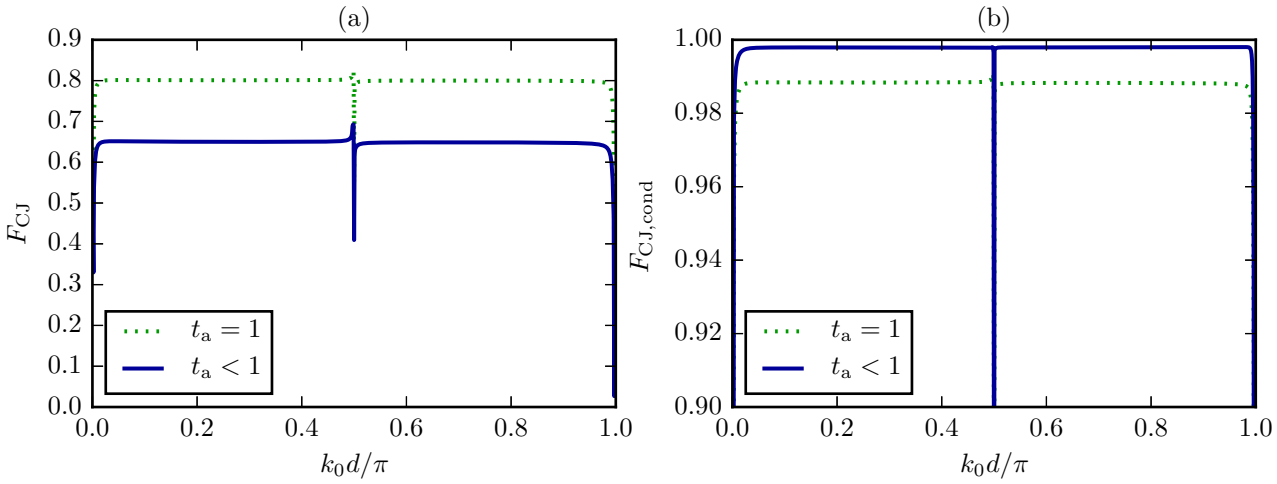

FIG. S10. Comparison of (a) unconditional and (b) conditional Choi-Jamiolkowski fidelities for the dual-V scheme plotted as functions of the interatomic spacing d times the photon wave vector k_0 for fixed number of atoms $N = 1000$ and $\Gamma_{1\mathrm{D}}/\Gamma = 0.5$. For storage and retrieval, we use the discretized storage and retrieval kernels derived in Sec. 5.4.

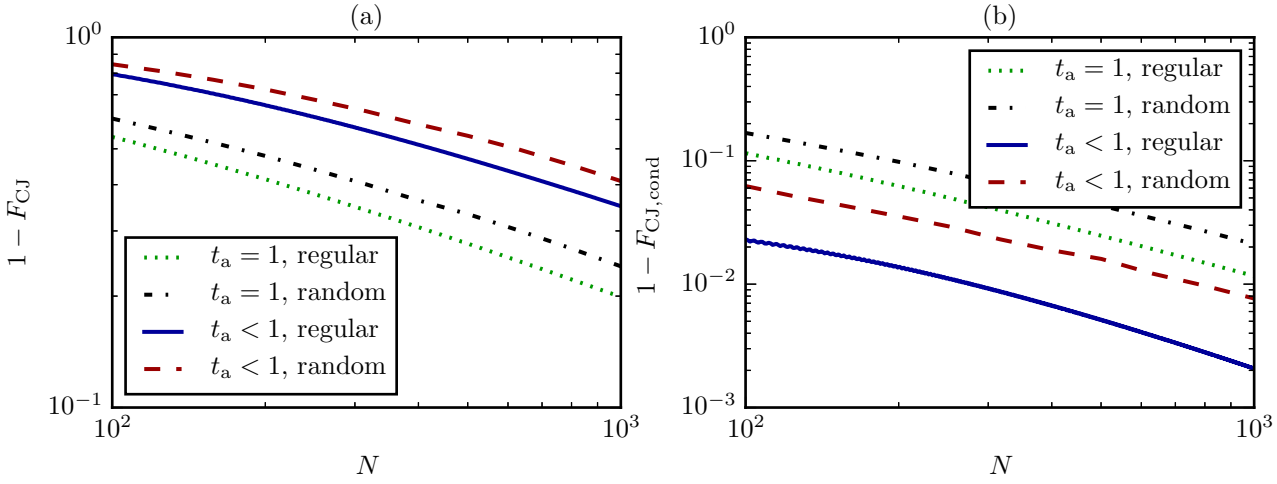

FIG. S11. Comparison of (a) unconditional and (b) conditional Choi-Jamiolkowski fidelities for the dual-V scheme with different placement of the atoms (regular or random) plotted as functions of the number of atoms N with fixed $\Gamma_{1\mathrm{D}}/\Gamma = 0.5$. The regularly placed atoms have have positions $z_j = jd$ for $d = 0.266\pi/k_0$ and $0 \leq j \leq N-1$. The positions of the randomly placed atoms are chosen from the uniform distribution over the whole ensemble and then sorted in increasing order. For random placement, we average over 1000 ensemble realizations. For storage and retrieval, the fully discrete model of Sec. 5.3 is used. For regular placement, it gives the same results as the discretized storage and retrieval kernels derived in Sec. 5.4, but for random placement, the fully discrete model has significant deviations from the discretized storage and retrieval kernels as shown in Fig. S7. The optimal Δ_{c} and $\tilde{\sigma}$ (width of the stored Gaussian spin wave) are found by doing numerical optimization using the discretized storage and retrieval kernels, since the fully discrete model is much more computationally demanding.

[S7] G. Bertocchi, O. Alibart, D. B. Ostrowsky, S. Tanzilli, and P. Baldi, Journal of Physics B: Atomic, Molecular and Optical Physics **39**, 1011 (2006).
[S8] M. Bradford, K. C. Obi, and J.-T. Shen, Phys. Rev. Lett. **108**, 103902 (2012).
[S9] D. E. Chang, A. H. Safavi-Naeini, M. Hafezi, and O. Painter, New Journal of Physics **13**, 023003 (2011).
[S10] T. Caneva, M. T. Manzoni, T. Shi, J. S. Douglas, J. I. Cirac, and D. E. Chang, New Journal of Physics **17**, 113001 (2015).
[S11] A. V. Gorshkov, A. André, M. D. Lukin, and A. S. Sørensen, Phys. Rev. A **76**, 033805 (2007).